iScience

Article

$GABA_AR$-δ-subunit mediates increased GABAergic inhibition in cardiac DMV neurons after high-fat diet

Graphical abstract

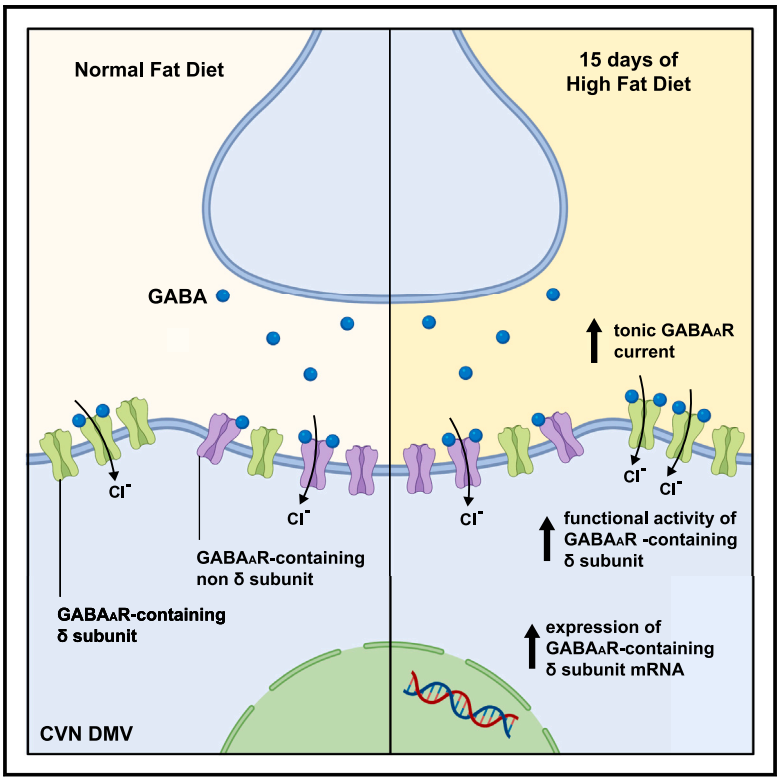

Authors

Yoko Brigitte Wang, Kaylie E. Dow, Carie R. Boychuk

Correspondence

boychukc@missouri.edu

In brief

Natural sciences; Biological sciences; Physiology; Neuroscience

Highlights

- Fifteen-day HFD induced increase of tonic $GABA_AR$ current specific to CVN^{DMV}
- Expression of $GABA_AR$-containing δ subunit mRNA in CVN^{DMV} increased after 15-day HFD
- $GABA_AR$-containing δ subunit mediates HFD-induced tonic $GABA_AR$ current in CVN^{DMV}

Wang et al., 2025, iScience *28*, 112268
April 18, 2025
https://doi.org/10.1016/j.isci.2025.112268

CellPress

iScience

CellPress
OPEN ACCESS

Article

$GABA_AR$-δ-subunit mediates increased GABAergic inhibition in cardiac DMV neurons after high-fat diet

Yoko Brigitte Wang,[1,2] Kaylie E. Dow,[1,2] and Carie R. Boychuk[1,2,3,*]
[1]Dalton Cardiovascular Research Center, University of Missouri, Columbia, MO, USA
[2]Department of Biomedical Sciences, College of Veterinary Medicine, University of Missouri, Columbia, MO, USA
[3]Lead contact
*Correspondence: boychukc@missouri.edu
https://doi.org/10.1016/j.isci.2025.112268

SUMMARY

Activity of cardiac-projecting neurons in the dorsal motor nucleus of the vagus (CVN^{DMV}) is vital in cardiac reflexes contributing to maintaining cardiovascular health. However, how this population adapts to metabolic challenges, such as high-fat diet (HFD), is unclear. This study aimed to identify neuroplasticity changes induced by HFD in CVN^{DMV}. Using whole-cell patch-clamp electrophysiology, we found that 15-day HFD feeding increased tonic, but not phasic, gamma-aminobutyric acid type A ($GABA_A$) inhibitory neurotransmission, exclusive to CVN^{DMV}. Single-cell quantitative reverse-transcription PCR (scRT-qPCR) analysis revealed a higher number of CVN^{DMV} expressing $GABA_A$ receptor δ-subunit ($GABA_A$(δ)R) in HFD compared to normal fat diet (NFD). Deletion of $GABA_A$(δ)R in ChAT-positive motor neurons abolished HFD-induced increased tonic $GABA_A$ neurotransmission in CVN^{DMV}. Altogether, this evidence suggests that CVN^{DMV} exhibits early onset HFD-induced increased GABAergic neurotransmission, likely mediated by $GABA_A$(δ)R. This increased inhibitory tone could explain previously reported reduced cardiac vagal motor output, thus contributing to poor cardiometabolic health after HFD.

INTRODUCTION

Cardiac-projecting vagal motor neurons (CVNs) in the brainstem play a vital role in maintaining cardiac homeostasis by slowing cardiac activity (i.e., cardioinhibition), which when active is cardioprotective in a number of homeostatic disturbances.[1,2] Conversely, decrease in vagal motor output increases risk of cardiovascular disease and mortality,[3,4] making maintenance of proper CVN activity critical to overall health. Of note, reduction in cardiac vagal output is evident in the presence of metabolic challenges, including obesity—a growing public health burden and a key risk factor of cardiovascular diseases.[5,6] Mechanistic studies in animal models of obesity, induced by high fat diet (HFD) exposure, also provide evidence of early dampening of cardiac vagal control,[7–9] even before onset of weight gain and which persists as long as animals were on HFD.[10] Together, these investigations suggest that metabolic perturbations like HFD can reduce CVN activity. Although reduced vagal activity is of central origin,[10] the neuromechanistic underpinning of HFD-induced dampening of CVN activity remains unclear.

Despite residing in two major brainstem nuclei, nucleus ambiguus (NA) has received the majority of attention into the role of central CVNs in cardiac physiology. However, the second vagal nucleus, dorsal motor nucleus of the vagus (DMV), also contains a population of CVNs that regulate cardiac nodal cells[10–13] and myocytes.[14,15] While little work has been done on these cardiac-projecting neurons in DMV (CVN^{DMV}) in disease states, evidence exists establishing CVN^{DMV} as disease modifiers since their activation improves cardiac function in animal models of heart failure, chronic intermittent hypoxia, and hypertension.[16,17] Importantly, CVN^{DMV} may serve as a key signaling locus linking metabolic perturbations to the cardiac system, since DMV and the circuits that project to this region respond to metabolic cues,[18–20] are impacted by HFD,[21–23] and facilitate heart-gut interorgan interaction in ischemia and exercise.[24] Although anatomical location and physiological function of CVN^{DMV} indicate that they may mediate effects of metabolic challenges to cardiac vagal motor output, their plasticity adaptions to HFD remain to be determined.

Inhibitory gamma-aminobutyric acid (GABA) neurotransmission perturbations are noted throughout the central nervous system as contributing to metabolic pathophysiology.[25,26] For example, long-term HFD exposure during the perinatal period increased excitatory drive to presynaptic GABAergic synaptic terminals on gastric-projecting DMV neurons that associated with decreased parasympathetic outflow to the stomach.[22] However, GABAergic neurotransmission in DMV is mediated by two signaling modalities, tonic and phasic (i.e., presynaptic), which is predicted by the subunit composition of the heteropentameric membrane spanning $GABA_A$ receptors

($GABA_AR$s)[27–30] and the dynamic mobility of receptors in and out of the membrane.[31] Despite evidence of changes in presynaptic release of GABA after perinatal HFD, other studies indicate DMV neurons increased tonic, but not phasic, GABAergic current after metabolic challenges such as experimentally induced type 1 diabetes and long-term perinatal HFD.[21,32] Among several critical subunits, $GABA_AR$s containing the δ-subunit can contribute to increases in tonic current in response to metabolic adaptation,[32] and at least protein expression of the δ-subunit is increased in other vagal motor output brain regions after HFD.[10] Unfortunately, few tools previously existed to selectively target $GABA_AR$s containing the δ-subunit, limiting the ability to make strong associations with disruption in neurophysiology and the δ-subunit. Additionally, no study to date examined whether increased inhibition of $GABA_AR$s containing the δ-subunit associates with early (<14 days) disease progression in adulthood, when mice do not demonstrate robust changes in weight or glucose tolerance.[10] Therefore, we hypothesized that HFD increases tonic inhibitory current provided by $GABA_AR$ containing the δ-subunit that may lead to a reduced cardiac parasympathetic outflow early in disease (<14 days) when exposure occurs during adulthood. To test this hypothesis, we used whole-cell patch-clamp electrophysiology, single cell quantitative reverse-transcription PCR (scRT-qPCR) and two novel transgenic mouse models.

RESULTS

Fifteen-days of HFD increases tonic but not phasic $GABA_AR$ neurotransmission in CVN^{DMV}

Since our previous report demonstrated robust inhibition of cardiac vagal motor output after 15 days of HFD,[10] we first investigated whether acute HFD, after three or fifteen days, impacted GABAergic neurotransmission in CVN^{DMV}. Voltage-clamp recordings were performed on CVN^{DMV} neurons retrogradely labeled with rhodamine (Figure 1B). Confirmation of location in DMV and colocalization with ChAT were done through post-hoc recovery of biocytin (Figure 1C), and recordings were done for both tonic and phasic $GABA_AR$s (Figure 1D). Bicuculline methiodide (30 μM), a general antagonist of $GABA_AR$, was applied to determine tonic $GABA_AR$ current amplitude in CVN^{DMV} (Figure 1E). CVN^{DMV} from 15D HFD animals had a significantly higher tonic current density compared to normal fat diet (NFD) (HFD_{15D} vs. NFD = 1.32 ± 0.14 vs. 0.78 ± 0.12 pA/pF, $n_{NFD\ cardiac}$ = 11 cells/6 mice, $n_{15D\ HFD\ cardiac}$ = 12 cells/6 mice, one-way ANOVA, Tukey's post-hoc test; p = 0.01) and 3D HFD (HFD_{3D}: 0.42 ± 0.08 pA/pF, $n_{3D\ HFD\ cardiac}$ = 10 cells/5 mice, one-way ANOVA, Tukey's post-hoc test; $p < 0.0001$) (Figure 1F). There was no difference between 3D HFD CVN^{DMV} and NFD (one-way ANOVA, Tukey's post-hoc test; p = 0.16). Control groups for 3D and 15D NFD were combined as they were not different ($NFD_{3D\ vs\ 15D}$ = 0.74 ± 0.33 vs. 0.80 ± 0.10 pA/pF, $n_{3D\ NFD\ cardiac}$ = 3 cells/2 mice, $n_{15D\ NFD}$ = 8 cells/4 mice, two-tailed unpaired Student's t test; p = 0.84). There were no differences in cell capacitance between CVN^{DMV} from NFD or HFD groups (NFD vs. HFD_{3D} vs. HFD_{15D} = 43.88 ± 6.76 vs. 44.51 ± 4.30 vs. 37.20 ± 3.28 pF, one-way ANOVA, Tukey's post-hoc test, p = 0.72), indicating that increases in tonic current after HFD are not related to large changes in cell size.

Since DMV is also populated by neurons with other peripheral organ projections that receive prominent GABAergic neurotransmission,[33] we tested whether increased tonic current density after 15D HFD is specific to CVN^{DMV}. Voltage-clamp recordings were performed on gastric-projecting and unlabeled DMV neurons. Tonic current density of 15D HFD CVN^{DMV} remained significantly higher compared to non-cardiac DMVs in NFD or HFD groups (NFD_{other} = 0.79 ± 0.14 pA/pF, p = 0.02; HFD_{other} = 0.80 ± 0.09 pA/pF, p = 0.03; $n_{NFD\ other}$ = 8 cells/5 mice, $n_{HFD\ other}$ = 8 cells/4 mice, one-way ANOVA, Tukey's post-hoc test). There was no difference in tonic current density between 15D NFD cardiac and non-cardiac DMV groups ($NFD_{15D\ cardiac\ vs\ NFD_{other}}$ = 0.78 ± 0.10 vs. 0.79 ± 0.14 pA/pF; one-way ANOVA, Tukey's post-hoc test, $p \geq 0.99$), or with 15D HFD non-cardiac DMV (HFD_{other} = 0.80 ± 0.10 pA/pF, one-way ANOVA, Tukey's post-hoc test, $p \geq 0.99$). No significant difference was found between non-cardiac NFD and HFD groups ($NFD_{other\ vs\ HFD_{other}}$ = 0.79 ± 0.14 vs. 0.80 ± 0.10 pA/pF, one-way ANOVA, Tukey's post-hoc test, $p > 0.99$). This suggests that the influence of acute HFD on tonic $GABA_AR$ current in adult mice was selective to cardiac-projecting DMV neurons.

We also determined if 15D HFD feeding affects phasic GABAergic neurotransmission. However, no differences were observed on any phasic current components in CVN^{DMV} between NFD, 3D HFD and 15D HFD, such as in sIPSC frequency (NFD vs. HFD_{3D} vs. HFD_{15D} = 6.41 ± 2.35 vs. 3.68 ± 1.07 vs. 3.48 ± 1.04 Hz, p = 0.36; one-way ANOVA, Tukey's post-hoc test, Figure 1H), amplitude (NFD vs. HFD_{3D} vs. HFD_{15D} = 28.17 ± 2.34 vs. 28.39 ± 2.96 vs. 28.16 ± 2.18 pA, p = 0.99; one-way ANOVA, Tukey's post-hoc test, Figure 1I) and decay time (NFD vs. HFD_{3D} vs. HFD_{15D} = 7.07 ± 0.62 vs. 7.30 ± 0.98 vs. 6.73 ± 0.43 ms, p = 0.82; one-way ANOVA, Tukey's post-hoc test, Figure 1J). Altogether, exposure of HFD for 15 but not 3 days affects tonic but not phasic GABA current, exclusively in CVN^{DMV}.

Fifteen-days of HFD increases tonic $GABA_AR$ neurotransmission from receptors containing the δ-subunit in CVN^{DMV}

A robust theoretical framework implicates $GABA_AR$s containing the δ-subunit as critical in generating tonic current.[34,35] To test whether $GABA_AR$s containing the δ-subunit are involved in the impact of HFD on CVN^{DMV} tonic $GABA_AR$ current, we used a unique CRISPR-Cas9-made knock in/chemogenetic transgenic mouse line (δ*KI). This mouse line harbors a point mutation at the membrane-spanning domain (M2) of the δ-subunit located on exon 8, rendering any $GABA_AR$s containing the δ-subunit resistant to the general $GABA_AR$ antagonist, picrotoxin (PTX; Figure 2A).[36] To isolate tonic currents generated specifically by $GABA_AR$s containing the δ-subunit in δ*KI mice, we administered PTX (10 μM) to eliminate the activity of $GABA_AR$s without the δ-subunit, followed by bicuculline (BIC) (30 μM; Figure 2B). In this sequence, then, the tonic current eliminated by BIC application is due only to activity of $GABA_AR$s containing the δ-subunit. In these δ*KI mice, 15D HFD CVN^{DMV} had a significantly higher tonic current density in response to BIC (1.27 ± 0.19 pA/pF;

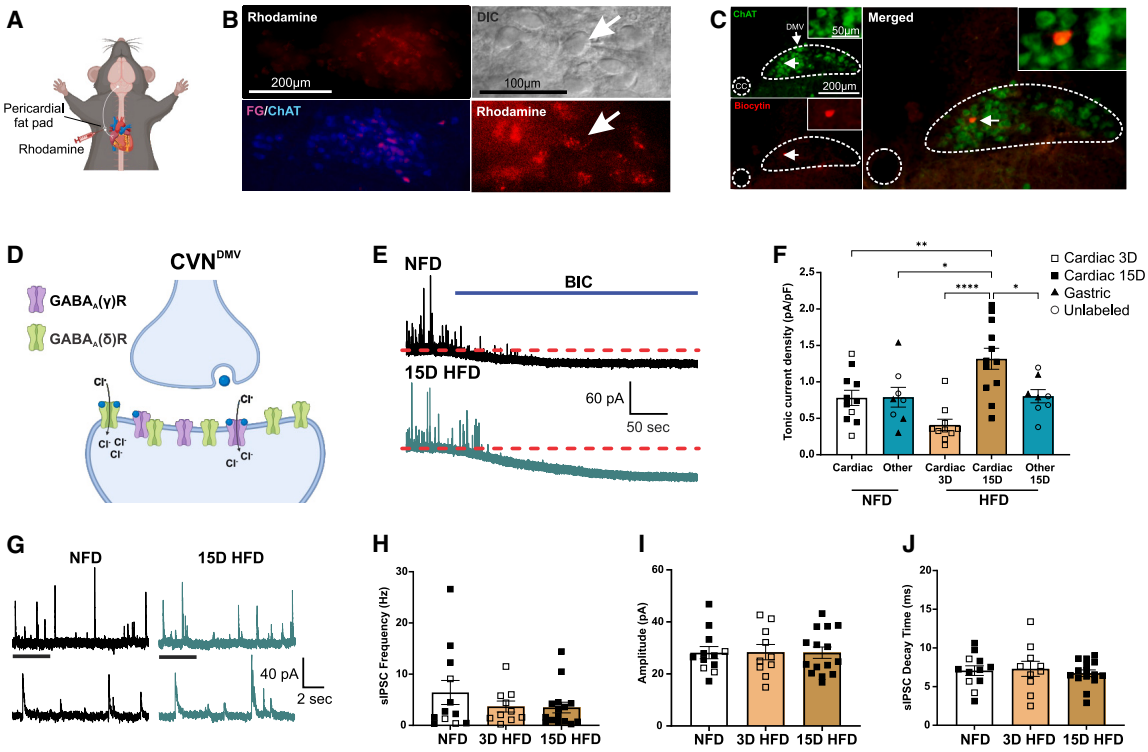

Figure 1. Increased of tonic GABAergic current after 15D high fat diet

(A) Illustration of retrograde cardiac injection.

(B) Representative image of CVN^{DMV} under differential inference contrast (top) and epifluorescence microscope (bottom).

(C) Representative images of biocytin and ChAT colocalization in recorded CVN^{DMV}.

(D) A diagram of GABAergic neurotransmission and distribution of $GABA_AR$ in synaptic junction.

(E) Representative traces of tonic GABAergic current before and after BIC application in NFD and 15D HFD groups; dashed red line indicate current holding baseline before BIC.

(F) Tonic current density of NFD and HFD groups in cardiac (□-3D, ■-15D) and non-cardiac (▲-15D gastric, ○-15D unlabeled) DMV neurons ($n_{NFD\ cardiac}$ = 11 cells from 6 mice, $n_{NFD\ other}$ = 8 cells from 5 mice, $n_{3D\ HFD\ cardiac}$ = 10 cells from 5 mice, $n_{15D\ HFD\ cardiac}$ = 12 cells from 9 mice, $n_{15D\ HFD\ other}$ = 8 cells from 4 mice, one-way ANOVA, F(4,44) = 8.572, $p_{NFD\ cardiac\ vs\ 15D\ HFD\ cardiac}$ = 0.01, $p_{NFD\ other\ vs\ 15D\ HFD\ cardiac}$ = 0.03, $p_{15D\ HFD\ cardiac\ vs\ 15D\ HFD\ other}$ = 0.04, $p_{3D\ HFD\ cardiac\ vs\ 15D\ HFD\ cardiac}$ = <0.0001).

(G) Representative traces of CVN^{DMV} sIPSC.

(H–J) Phasic GABAergic neurotransmission components: (H) sIPSC frequency, (I) amplitude, and (J) sIPSC decay time (*NS*, one-way ANOVA). Data are represented as mean ± SEM. *NS*, not significant, $^*p \leq 0.05$, $^{****}p \leq 0.0001$. Tukey's post-hoc test was done for one-way ANOVA.

DIC, differential inference contrast; ChAT, choline acetyltransferase; CVN^{DMV}, cardiac-projecting vagal motor neuron; BIC, bicuculine; NFD, normal fat diet; HFD, high fat diet; sIPSC, spontaneous inhibitory postsynaptic current.

n = 5 cells/3 mice) compared to CVN^{DMV} from NFD mice (0.52 ± 0.16 pA/pF; *n* = 3 cells/2 mice; unpaired, two-tailed Student's t test, p = 0.035; Figure 2D). To further confirm the role of $GABA_ARs$ containing the δ-subunit, we recorded tonic activity of CVN^{DMV} from C57BL/6J mice before and after application to the $GABA_ARs$ containing the δ-subunit super agonist, 4,5,6,7-Tetrahydroisoxazolo[5,4-*c*]pyridin-3-ol hydrochloride (THIP; 3 μM). Upon bath application, 15D HFD CVN^{DMV} also possessed significantly higher tonic current density in response to THIP activation of $GABA_ARs$ containing δ-subunit (0.51 ± 0.22 pA/pF; *n* = 5 cells/2 mice) compared to CVN^{DMV} from mice on NFD (0.031 ± 0.06 pA/pF; *n* = 8 cells/4 mice; unpaired, two-tailed Student's t test, p = 0.024; Figure 2F). Together, these experiments provide robust evidence that tonic current density in CVN^{DMV} generated specifically from $GABA_ARs$ containing δ-subunit increased after 15 days of HFD consumption.

HFD induces increased $GABA_AR$-dependent GABAergic drive in CVN^{DMV}

Tonic GABAergic inhibition regulates neuronal excitability throughout the central nervous system,[37] and specifically within DMV.[30] To determine if HFD-induced increases in tonic GABAergic current impact CVN^{DMV} excitability, brain slices containing DMV were examined in current clamp configuration at 15D of diet. There were no significant differences in basic electrophysiological properties (Figure S1) under resting, normal ACSF conditions between NFD and 15D HFD animals, including membrane potential, input resistance and action potential firing. To determine if the relative contributions of fast synaptic neurotransmission were altered by 15D HFD, action potential generation was examined before and after synaptic signaling was blocked with both CNQX/AP5 (10 μM), the ionotropic glutamate receptors antagonists, and BIC (30 μM)

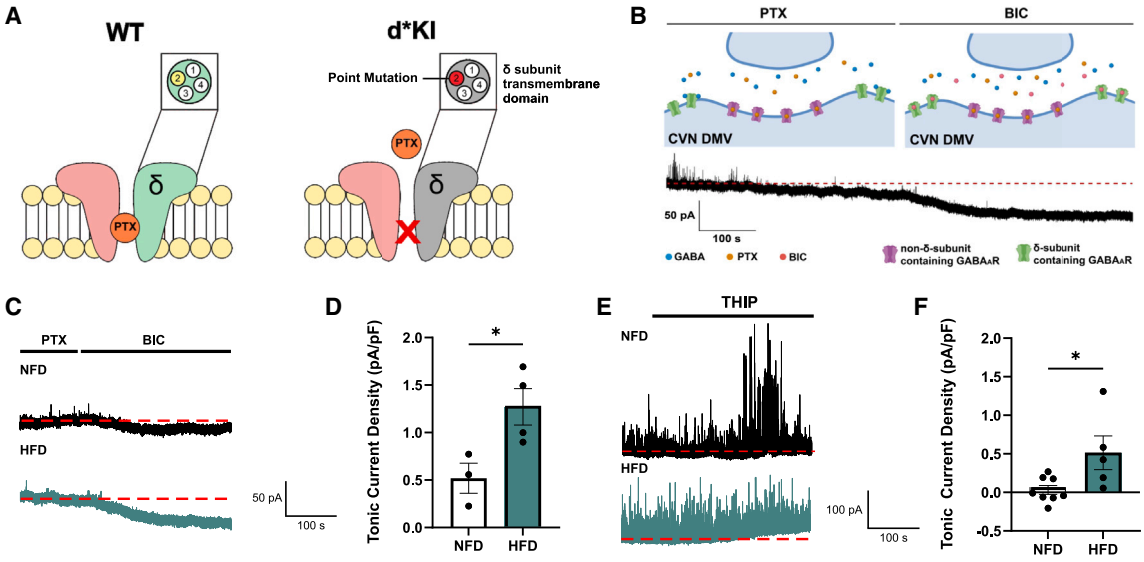

Figure 2. Increased $GABA_AR$ containing δ-subunit contributions are responsible for elevated tonic $GABA_AR$ currents after 15D high fat diet in CVN^{DMV}

(A) Schematic side view illustrating the position of PTX in the pore of a WT $GABA_AR$ and the lack of binding of PTX in δ*KI $GABA_AR$.

(B) Representative trace of tonic currents illustrating the sequential administration of PTX and BIC in CVN^{DMV} from δ*KI mice.

(C) Representative trace of GABAergic current during application of PTX and BIC in 15D NFD and HFD.

(D) BIC-sensitive tonic current density in CVN^{DMV} from δ*KI mice fed either NFD or 15D HFD after application of PTX to isolate $GABA_AR$ containing δ-subunit (n_{NFD} = 3 cells from 2 mice, N_{HFD} = 4 cells from 3 mice; unpaired, two-tailed Student's t test; p = 0.035, t = 2.867, df = 5).

(E) Representative traces of tonic GABAergic current density before and after THIP application in NFD and 15D HFD of C57/Bl6J mice; dashed red line indicate current holding before THIP application.

(F) Tonic current density of NFD and HFD in CVN^{DMV} neurons (n_{NFD} = 8 cells from 4 mice, n_{HFD} = 5 cells from 2 mice, unpaired, two-tailed Student's t test, p = 0.024, t = 2.621, df = 11). Data are represented as mean ± SEM. *$p \leq 0.05$.

NFD, normal fat diet; HFD, high fat diet; GABA, gamma aminobutyric acid; THIP, 4,5,6,7-tetrahydroisoxazolo[5,4-*c*]pyridin-3-ol hydrochloride; PTX, picrotoxin; BIC, bicuculine.

(Figure S2A). In NFD, a total synaptic blockade significantly reduced the number of action potentials evoked by CVN^{DMV} compared to normal ACSF conditions (ACSF vs. total blockade = 4.92 ± 0.95 vs. 2.83 ± 0.74, n_{NFD} = 9 cells/6 mice, repeated measures two-way ANOVA, Sidak post-hoc test, p = 0.04, Figure S2B). In contrast, no significant change was observed in the number of evoked action potentials in HFD before and after total synaptic blockade (ACSF vs. total blockade = 5.87 ± 1.04 vs. 5.39 ± 1.30, n_{HFD} = 9 cells/8 mice, repeated measures two-way ANOVA, Sidak post-hoc test, p = 0.39, Figure S2C). These results indicate that while CVN^{DMV} after 15D HFD may have elevated excitability compared to NFD, the balance of fast synaptic neurotransmission must compensate for this increased excitability since there were no overt differences under normal ACSF conditions.

Thus, to further investigate whether this altered balance between fast neurotransmission and overall excitability was related to decreased glutamatergic tone or increased GABAergic tone, we measured action potentials evoked before and after pharmacological blockade in current clamp. Using glutamatergic blockade again with CNQX/AP5 (Figure 3A), both NFD and 15D HFD CVN^{DMV} showed a significant reduction of action potentials elicited during step current injection ($NFD_{before\ vs\ CNQX/AP5}$ = 4.93 ± 0.95 vs. 3.78 ± 0.90, p = 0.02, Figure 3B; $HFD_{15D\ before\ vs\ CNQX/AP5}$ = 5.87 ± 1.04 vs. 4.63 ± 1.01, p = 0.03; Figure 3C; repeated measures two-way ANOVA, Sidak post-hoc test). The change of ionotropic glutamatergic drive, represented by area under the curve (AUC), was not different between the two groups ($AUC_{NFD\ vs\ HFD15D}$ = −311.1 ± 100.8 vs. −350.0 ± 127.9 a.u., two-tailed unpaired Student's t test, p = 0.81, Figure 3D). Finally, CVN^{DMV} from animals on HFD almost uniformly decreased the number of action potentials at 250 pA current injection (~89%; Figure 3I) similar to CVN^{DMV} from animals on NFD (~78%; Chi-square test; p = 0.5; Figures 3I and 3J). Therefore, under *ex vivo* conditions, the contribution of glutamatergic signaling to overall CVN^{DMV} excitability remained similar between NFD and HFD.

We then examined the number of action potentials generated after $GABA_AR$ blockade in CVN^{DMV} (Figure 3E). No difference was found in the number of action potentials generated before and after BIC application of CVN^{DMV} from NFD ($NFD_{before\ vs\ BIC}$ = 3.78 ± 0.90 vs. 2.83 ± 0.74, repeated measures two-way ANOVA, Sidak post-hoc test, p = 0.81, Figure 3F), similar to previous reports.[38] However, in CVN^{DMV}s from 15D HFD animals, antagonizing $GABA_AR$-dependent GABAergic neurotransmission increased the number of evoked action potentials ($HFD_{before\ vs\ BIC}$ = 4.63 ± 1.01 vs. 5.39 ± 1.30, repeated measures two-way ANOVA, Sidak post-hoc test, p = 0.005, Figure 3G) and

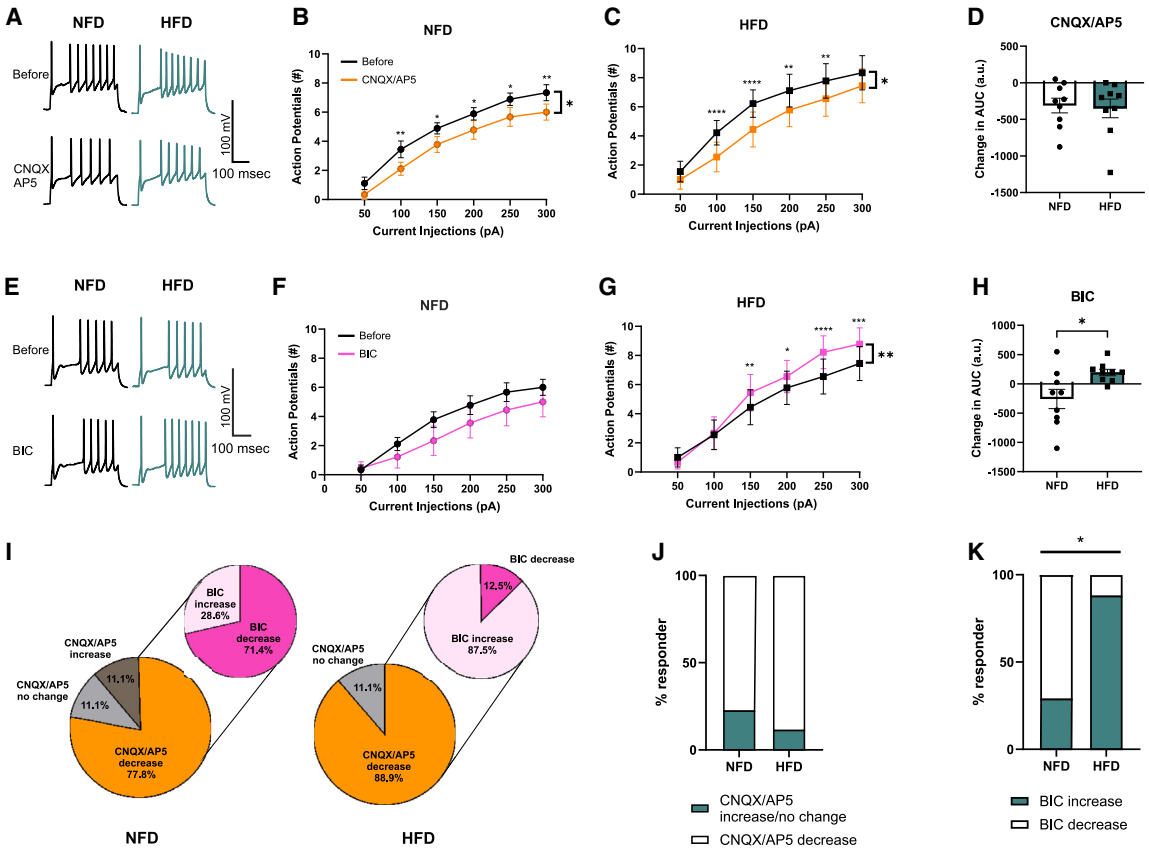

Figure 3. Increased GABAergic neurotransmission drives in CVN^{DMV} after 15D high fat diet

(A) Representative traces of NFD and HFD CVN^{DMV} action potentials before (nACSF) and after CNQX/AP5. Action potentials evoked before and after CNQX/AP5 in B) NFD (●, n = 9 cells from 6 mice; repeated measures two-way ANOVA: $F_{current}$ (5, 40) = 171.7, $p < 0.0001$; $F_{CNQX/AP5}$ (1, 8) = 9.416, $p = 0.02$; F interaction (5, 40) = 0.2940, $p = 0.91$) and C) HFD (■, n = 9 cells from 8 mice; repeated measures two-way ANOVA: $F_{current}$ (5, 40) = 80.6, $p < 0.0001$; $F_{CNQX/AP5}$ (1, 8) = 7.554, $p = 0.03$; F interaction (5, 40) = 2.021, $p = 0.096$).

(D) Changes of area under the curve after CNQX/AP5 (*NS*, unpaired, two-tailed Student's t test).

(E) Representative traces of NFD and HFD CVN^{DMV} action potentials before (CNQX/AP5) and after BIC.

(F and G) Action potentials evoked before and after BIC in (F) NFD (*NS*; repeated measures two-way ANOVA) and (G) HFD (repeated measures two-way ANOVA: $F_{current}$ (5, 40) = 75.24, $p < 0.0001$; F_{BIC}(1, 8) = 14.34, $p = 0.005$; F interaction (5, 40) = 7.513, $p < 0.0001$).

(H) Changes of the area under the curve after BIC (unpaired, two-tailed Student's t test; $p = 0.02$, t = 2.613, df = 16).

(I) Percentage of cells based on response to CNQX/AP5 and BIC in NFD and HFD.

(J and K) The proportion of cells (J) with decreased response to CNQX/AP5 (Chi-square test, $p = 0.05$) and (K) with increased response to BIC (Chi-square test, $p = 0.02$) in NFD and HFD groups. Data are represented as mean ± SEM. *NS*, not significant, $^{*}p \leq 0.05$, $^{**}p \leq 0.01$. Sidak post-hoc test was done for repeated measures two-way ANOVA.

NFD, normal fat diet; HFD, high fat diet; CNQX, cyanquaxaline; AP5, D-2-amino-5-phosphopentanoate; BIC, bicuculine; AUC, area under the curve.

the change in ionotropic GABAergic drive in CVN^{DMV} from HFD animal as described by AUC was significantly greater compared to NFD ($AUC_{NFD\ vs\ HFD} = -258.3 \pm 164.3$ vs. 194.4 ± 55.08 a.u., unpaired, two-tailed Student's t test, $p = 0.02$, Figure 3H). Finally, CVN^{DMV} from animals on HFD almost uniformly increased the number of action potentials at 250 pA current injection (~88%; Figure 3I) compared to CVN^{DMV} from animals on NFD (~29%). This shift in response profile was significantly different (Chi-square test; $p = 0.02$; Figures 3I and 3K). Taken together, these data suggest that CVN^{DMV} likely are hyperexcitable after 15D of HFD feeding and this is masked under normal conditions by a larger influence of $GABA_A$R-dependent GABAergic neurotransmission.

Expression of $GABA_A$R-δ-subunit increased in CVN^{DMV} after HFD

Assembly of specific subunits is critical to the diversity of $GABA_A$R signaling[39,40]; and tonic GABA current is typically generated by $GABA_A$R consisting of two α- and two β-subunits paired with δ-subunit.[35] Therefore, we investigated whether an increased tonic GABAergic current in CVN^{DMV} after 15D HFD is driven by increased expression of δ-subunit containing $GABA_A$Rs. Individual CVN^{DMV} from NFD and 15D HFD-fed mice were profiled for transcript expression of eight $GABA_A$R subunits, α1-5 (*gabra1-5*), δ (*gabrd*), and γ1-2 (*gabrg1-2*), using scRT-qPCR (Figure 4A). Expression of two housekeeping genes, β-actin and glyceraldehyde 3-phosphate dehydrogenase (GAPDH), were present in all

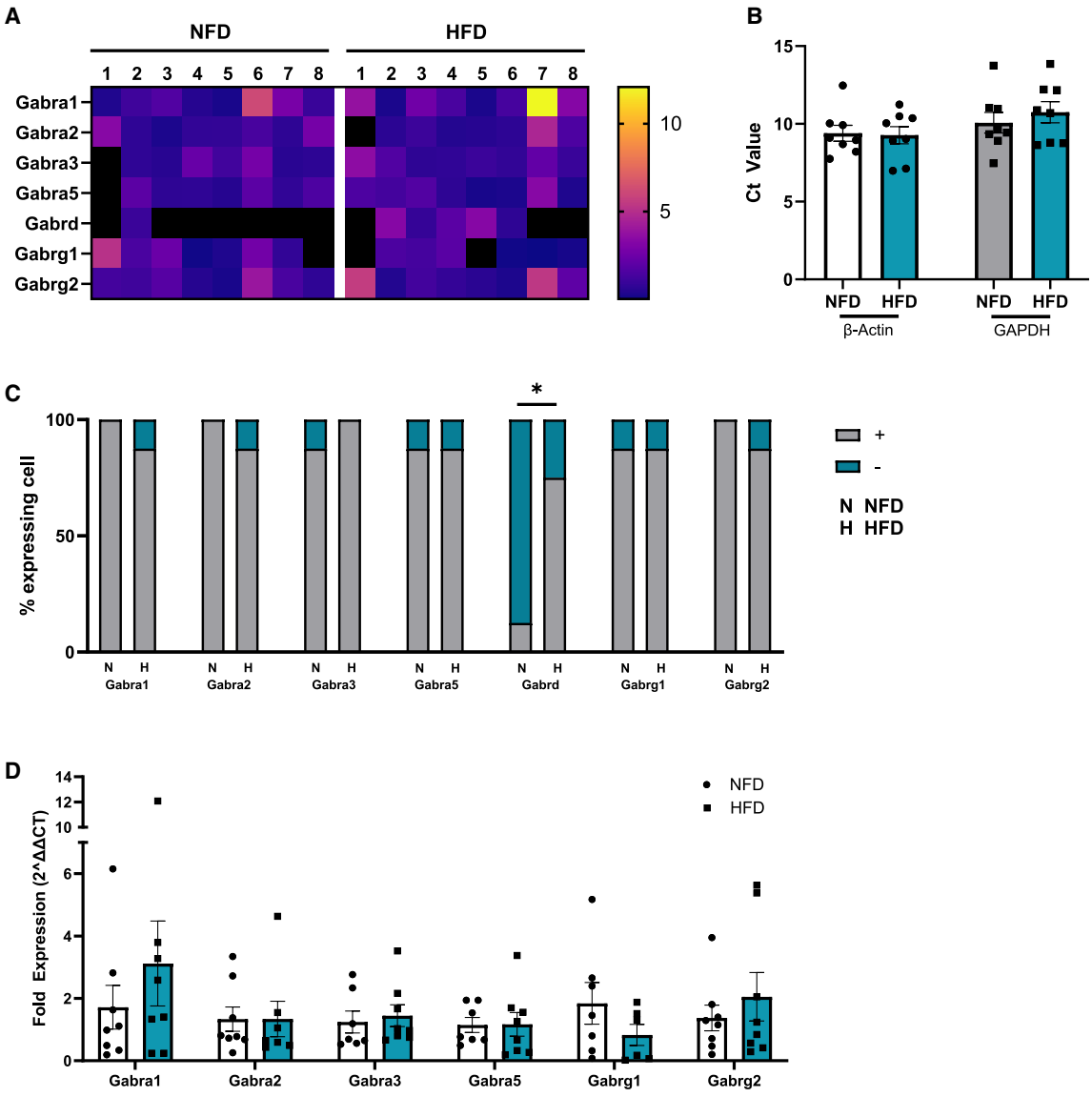

Figure 4. mRNA expression profile of $GABA_AR$ subunits in CVN^{DMV}

(A) Heatmap of $GABA_AR$ subunits fold expression in NFD and 15D HFD CVN^{DMV}, black square denotes undetected Ct Values (n_{NFD} = 8 cells from 4 mice, n_{HFD} = 8 cells from 5 mice).

(B) Ct Values of housekeeping genes (*NS*, two-way ANOVA).

(C) Proportion of cells expressing $GABA_AR$ subunits (Chi-square test; p_{Gabard} = 0.01).

(D) Fold expression of $GABA_AR$ subunits (*NS*; unpaired two-tailed Student's t Test). Data are represented as mean ± SEM. *NS*, not significant, $^*p \leq 0.05$. NFD, normal fat diet; HFD, high fat diet.

CVN^{DMV} samples and they were not different in NFD or HFD animals (β-$actin_{NFD\ vs\ HFD}$ = 9.39 ± 0.52 vs. 9.27 ± 0.55; $GAPDH_{NFD\ vs\ HFD}$ = 10.07 ± 0.66 vs. 10.75 ± 0.68; n_{NFD} = 8 cells/4 mice, n_{HFD} = 8 cells/5 mice, two-way ANOVA, Tukey's post-hoc test, p = 0.81, Figure 4B). This indicates that 15D HFD does not alter mRNA transcription in general. Only one out of eight CVN^{DMV} from NFD but five out of eight CVN^{DMV} from HFD group produced a detectable CT value for *gabrd* mRNA expression. This represented an increased proportion of CVN^{DMV} expressing $GABA_AR$ containing δ-subunit in HFD_{15D} (~62.5%) compared to NFD (~12.5%; Chi-square test, p = 0.01, Figure 4C). By contrast, there were no differences in either the proportion of cells or fold expression of other subunits between NFD and 15D HFD (Figure 4C and 4D). Also, no expression of α4 subunit was detected in any sample regardless of diet. Therefore, our results suggest that an increased number of CVN^{DMV} expressing $GABA_AR$-δ-subunit transcripts may play a role in increased tonic GABAergic current after 15D HFD.

Deletion of $GABA_AR$-δ-subunit mitigates the effect of HFD on CVN^{DMV} activity

To determine if increased transcription of the $GABA_AR$-δ-subunit impacts the role of HFD to increase inhibition, we performed whole-cell patch-clamp electrophysiology on CVN^{DMV} from ChAT-δ-null mice that lack $GABA_AR$-δ-subunit in their ChAT-positive motor neurons.[10] Qualitative immunohistochemical imaging confirmed that ChAT-δ-null had reduced $GABA_AR$-δ-subunit expression compared to mice with a floxed $GABA_AR$-δ-subunit cassette (Figure S3B). Knock down of δ-subunits in CVN^{DMV} was also confirmed with application of a low concentration of gabazine, a well-established method to identify tonic current generated by $GABA_AR$ that do not contain the δ-subunit.[34,41–43] As expected, CVN^{DMV} from ChAT-δ-null mice had significantly higher gabazine-sensitive tonic currents compared to wild-type (WT) littermates (ChAT-δ-null vs. WT = 0.66 ± 0.12 vs. 0.06 ± 0.04 pA/pF, n_{WT} = 8 cells/5 mice, n_{ChAT} = 8 cells/5 mice, unpaired, two-tailed Student's t test, p = 0.0009, Figure S3C). However, there was no robust difference in firing frequency, resting membrane potential, input resistance, and action potentials evoked under normal ACSF (Figures S3D–S3J).

To determine if the impact of 15D HFD required the presence of $GABA_AR$-δ-subunit, electrophysiological experiments to examine the impact of $GABA_AR$s on CVN^{DMV}s were then repeated in ChAT-δ-null mice either on NFD or HFD. When BIC was applied to CVN^{DMV} from ChAT-δ-null mice on 15D NFD or HFD (Figure 5A), both groups showed no difference in tonic GABAergic current density (0.91 ± 0.16 vs. 0.74 ± 0.09 pA/pF, n_{NFD} = 6 cells/5 mice, n_{HFD} = 7 cells/5 mice, unpaired, two-tailed Student's t test, p = 0.35, Figure 5B). This finding indicates that $GABA_AR$-δ-subunit facilitates tonic GABAergic neurotransmission in CVN^{DMV} and deletion of this subunit mitigates the effect of 15D HFD on increased tonic GABA current in CVN^{DMV}.

We also examined whether knockout of $GABA_AR$-δ-subunit rescues HFD-induced effects on CVN^{DMV} neuronal excitability. Under $GABA_AR$ blockade (Figure 5C), the number of action potentials evoked before and after BIC application was not different in CVN^{DMV} from NFD and 15D HFD animals ($NFD_{before\ vs\ BIC}$ = 5.69 ± 1.11 vs. 6.79 ± 1.33, p = 0.056, Figure 5D; $HFD_{15D\ before\ vs\ BIC}$ = 5.24 ± 0.99 vs. 5.71 ± 1.19, p = 0.18; Figure 5E; repeated measures two-way ANOVA, Sidak post-hoc test). The change in AUC was not different between NFD and 15D HFD (300.0 ± 123.4 vs. 121.4 ± 85.12 a.u., p = 0.26, unpaired, two-tailed Student's t test, Figure 5F), suggesting GABAergic drive between these dietary groups is similar. Furthermore, no change was observed when comparing action potentials evoked under normal ACSF and total synaptic blockade (Figures 5G–5I, $ACSF_{NFD\ vs\ HFD}$ = 5.45 ± 1.03 vs. 5.60 ± 0.96, p = 0.89; Figure 5H; total $block_{NFD\ vs\ HFD}$ = 6.79 ± 1.33 vs. 5.71 ± 1.19, p = 0.33; Figure 5I; repeated measures two-way ANOVA, Sidak post-hoc test).

We acknowledge that CVN^{DMV} from ChAT-δ-null mice on NFD exhibited more excitability after BIC application (Figure 5D), similar to C57BL/6J mice on HFD. Besides $GABA_AR$, BIC can block small conductance Ca^{2+} activated K^+ (SK) channel[44–46] that increases intracellular Ca^{2+} resulting in prolonged afterhyperpolarization (AHP).[47] We conducted analysis of AHP amplitude to confirm if BIC-induced hyperexcitability in CVN^{DMV} from ChAT-δ-null mice regardless of diet was SK channel-dependent (Figure S4). We did not find any differences in AHP amplitudes between NFD and 15D HFD of C57BL/6J (17.87 ± 1.0 vs. 20.22 ± 0.72 mV, n_{NFD} = 7cells/6 mice, n_{HFD} = 7 cells/7 mice, unpaired, two-tailed Student's t test, p = 0.08, Figure S4B) or ChAT-δ-null (22.81 ± 1.09 vs. 23.84 ± 1.83 mV, n_{NFD} = 5 cells/5 mice, n_{HFD} = 5 cells/5 mice, one-way ANOVA, Tukey's post-hoc test, p = 0.93, Figure S4D). However, regardless of diet, ChAT-δ-null mice had larger AHP amplitudes compared to C57BL/6J mice (ChAT-δ-$null_{NFD}$ vs. C57BL/6J = 22.81 ± 1.09 vs. 17.87 ± 1.0 mV, p = 0.05; ChAT-δ-$null_{HFD}$ vs. C57BL/6J = 23.84 ± 1.83 vs. 17.87 ± 1.0 mV, p = 0.02, one-way ANOVA, Sidak post-hoc test, Figure S4D). Therefore, it is likely that the increased number of action potentials in ChAT-δ-null mice is a secondary effect of increased sensitivity of SK channels to BIC in the transgenic mouse line, and not related to HFD-induced alternations in SK channels. Together, our knockout data suggest that $GABA_AR$-δ-subunit is required in mediating the effect of acute HFD feeding on GABAergic neurotransmission plasticity in CVN^{DMV}.

DISCUSSION

Despite extensive evidence that HFD disrupts vagal signaling,[21,48,49] little is known about its impacts on central cardiac vagal motor circuits. Here, we demonstrate that HFD induced early onset (15 days) increases GABAergic neurotransmission in adult murine CVN^{DMV}. Using two novel transgenic mouse lines and traditional pharmacological approaches, this increase in $GABA_AR$ tonic inhibitory current after 15D HFD was mediated by a marked increase in signaling specifically from $GABA_AR$s containing the δ-subunit. Mechanistically, increased currents from $GABA_AR$s containing the δ-subunit likely resulted from an increase in mRNA expression of this subunit. This interpretation is further supported since knock down of the δ-subunit in motor neurons eliminated the impact of HFD on CVN^{DMV} electrophysiology. Overall, the present study revealed that short-term consumption of HFD elicits increased inhibitory, GABAergic signaling in CVN^{DMV} at least in part through increased transcription of the δ-subunit, making vagal hypoactivity during HFD a needed area of exploration in the role of HFD to impact cardiovascular regulation.

In the present study, CVN^{DMV} were more susceptible to acute HFD feeding compared to gastric or unlabeled DMV neurons since no changes were observed in tonic $GABA_AR$ current of the latter two populations. Previous reports confirm that hypoexcitability in other subpopulations of DMV motor neurons occurred as a result of HFD-induced plasticity.[21,22] However, these studies identified two alternative mechanisms of action: reduced glutamatergic signaling[22] and increased potassium currents.[21] Both these examinations exposed animals to HFD for 40+ days, and in relation to reduced glutamate signaling, these animals were exposed during the perinatal period. Taken together with the present work, these data suggest that not only the length but also the developmental period of HFD exposure is likely critical to determining the impact of HFD on vagal plasticity. Given the ability of DMV to impact exercise tolerance,[50] it remains possible that the effects of HFD on CVN^{DMV} could precipitate further abnormal signaling and, as disease

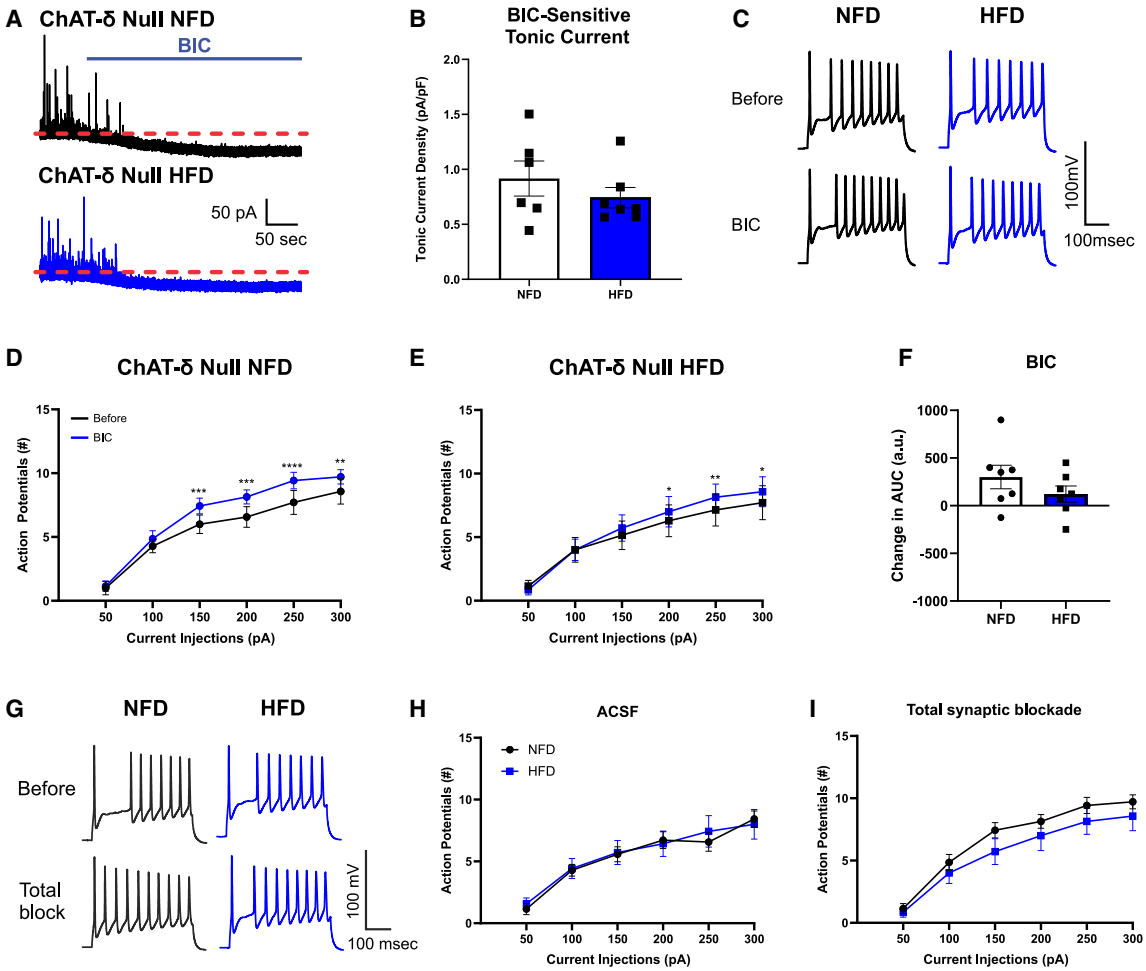

Figure 5. Deletion of $GABA_AR$-δ-subunit mitigates the effect of 15D high fat diet on CVN^{DMV} activity

(A) Representative traces of tonic GABAergic current before and after BIC application in NFD and 15D HFD ChAT-δ-null groups; dashed red line indicate current holding baseline before BIC.

(B) Tonic current density of NFD and HFD in CVN^{DMV} neurons (n_{NFD} = 6 cells from 5 mice, n_{HFD} = 7 cells from 5 mice, *NS*, unpaired, two-tailed Student's t test.).

(C) Representative traces of NFD and HFD CVN^{DMV} action potentials before (CNQX/AP5) and after BIC.

(D and E) Action potentials evoked before and after BIC in (D) NFD (*NS*; repeated measures two-way ANOVA) and (E) HFD (*NS*; repeated measures two-way ANOVA).

(F) Changes of area under the curve after BIC (*NS*; unpaired, two-tailed Student's t test).

(G) Representative traces of NFD and HFD CVN^{DMV} action potentials before (nACSF) and under total synaptic blockade (nASCF + CNQX/AP5 + BIC).

(H and I) Action potentials evoked before and under total synaptic blockade in (H) NFD (*NS*; repeated measures two-way ANOVA and (I) HFD (*NS*; repeated measures two-way ANOVA). Data are represented as mean ± SEM. *NS*, not significant, $*p \leq 0.05$, $**p \leq 0.01$, $***p \leq 0.001$. Sidak post-hoc test was done for repeated measures two-way ANOVA.

ChAT, choline acetyltransferase; NFD, normal fat diet; HFD, high fat diet; CNQX, cyanquaxaline; AP5, D-2-amino-5-phosphopentanoate; BIC, bicuculine; AUC, area under the curve.

progresses, begin to impact DMV neurons with other organ projections. These present data implicate CVN^{DMV} as a population where the effect of HFD is seen early in disease progression (before significant weight gain), and this impact is a distinct alteration in $GABA_AR$ tonic signaling and regulation.

This specificity is not surprising. It is true that most DMV neurons demonstrate robust tonic currents.[30,32,51] However, the current conceptual framework for circuit construction of DMV neurons includes a specificity in organ projection class, or "labeled lines."[52,53] Similarly, it is well established that upstream GABAergic neurons do not homogeneously and uniformly innervate all DMV neurons.[38,54,55] It is also not uncommon across different brain regions for cells in close appose with similar tonic currents to demonstrate differential impacts of any given experimental manipulation.[56] Finally, the limited availability of pharmacological interventions to isolate specifically the δ-subunit constrains our understanding of the exact nature of this subunit to generate tonic currents in DMV regardless of organ projection or health status. This latter point makes our use of a genetic knockdown of the δ-subunit and a knock-in mutant allowing us

to isolate δ-subunit currents distinctively novel. Taken together, despite demonstrating similar amplitudes of tonic currents, it is plausible that DMV neurons would demonstrate different impacts of any given experimental manipulation.

One potential mechanism of increased magnitude of tonic $GABA_AR$ current is an increase in GABA concentration in the synaptic and/or extracellular space. Studies using diet-induced-obesity and STZ-induced diabetes in rodents indicate that metabolic challenges can increase excitatory drive in presynaptic GABAergic neurons, thereby increasing GABA release from presynaptic terminals.[57,58] Additionally, in a classic tripartite synapse model, astrocytes orchestrate GABA concentration by regulating release and reuptake of GABA from the synaptic cleft or extracellular space,[35,59,60] and certainly, astrocytes in the brain can participate in the regulation of cardiovascular function.[61,62] HFD is also reported throughout several autonomic regulatory brain regions to induce astrocytic plasticity.[63–65] However, investigations into astrocytic contributions in the brainstem to autonomic function are primarily restricted to modulation of glutamatergic neurotransmission,[61,66,67] and therefore, little is known about astrocytic regulation of GABA concentration in DMV. However, tonic current generation in DMV neurons is eliminated after application of the sodium channel blocker, tetrodotoxin, implicating synaptic spillover (and not astrocyte transport) as the predominant source of extracellular GABA needed to generate tonic current.[51] Since in the present study, GABAergic phasic neurotransmission in CVN^{DMV} was not different between NFD and HFD groups, there is likely no change in presynaptic GABAergic activity under these conditions. Taken together, it is unlikely that increased tonic current amplitude is related to increased GABA concentration.

A second potential mechanism of increased $GABA_AR$ tonic current is a modification in postsynaptic receptor kinetic profile at the membrane, due to changes in synthesis, clustering, and phosphorylation of the receptors.[68,69] Since HFD increased the number of neurons robustly expressing the δ-subunit mRNA, it could be speculated that $GABA_AR$-δ-subunit protein synthesis is also increased, leading to more $GABA_AR$ containing-δ-subunit being assembled and transported to the membrane. Assembly of any given pentametric $GABA_AR$ is mainly dependent on two parameters: specific subunit abundance and the combinatorial principle of receptor construction.[70–72] This latter is critical since it did not appear that other subunit compositions were significantly altered. Therefore, it is possible that a higher δ-subunit abundance could be shifting the stoichiometry of $GABA_AR$ assembly toward an increase of δ-subunit in any given pentameric $GABA_AR$ arrangement,[73] or it shifts in favor of a specific subunit assembly.[74] Either way, this differential assembly could subsequently change the diversity of receptor types being transported to the membrane, with or without increasing the total number of receptors per se.

However, δ-subunit transcriptional expression does not always predict functional expression as defined by overall tonic current amplitude.[75,76] It is well established that $GABA_ARs$ are extensively regulated through post-translational mechanism(s), such as phosphorylation, to increase their plasma membrane expression.[77] Since tonic currents are maximally active in DMV neurons *ex vivo*,[78] even if ambient GABA concentration is increased, the number of functionally active $GABA_ARs$ at the plasma membrane would also need to increase to facilitate a functionally relevant increase in inhibition. Although typically $GABA_ARs$ in DMV do not respond to activation through increased functional expression, increased phosphorylation of $GABA_AR$ containing δ-subunits can increase tonic current by increased membrane expression.[79] Therefore, it is unlikely that increased tonic inhibition arises solely from increased transcription of the δ-subunit. Rather, increased tonic GABAergic current after 15D HFD may in part be due to postsynaptic adaptation in CVN^{DMV}, thereby further investigation is warranted to confirm hypotheses related to transcriptional and post-translational mechanisms of actions.

Differences in overall cell excitability were only seen under strict recordings conditions in the present study. This ''state-dependence'' is an established conceptual framework in our understanding of GABAergic signaling in DMV neurons,[80] suggesting that at this early stage in disease progression the impact of HFD is subtle. It is also well established that DMV neurons demonstrate seemingly contradictory findings on overall cell excitability with considerable diversity in the response of DMV neurons to antagonists of glutamate or GABA (tonic or otherwise), with these discrepancies suggested to predict upstream circuitry. For example, some DMV neurons respond to BIC application not with the predicted increase in firing frequency, but a decrease.[38] This has been suggested to occur because the antagonism of $GABA_ARs$ allows an exaggerated response from non-GABAergic mediated inhibitory influences. Since the vast majority of CVN^{DMV} from NFD animals demonstrated this decrease in excitability after BIC, it is interesting to speculate that CVN^{DMV} is largely influenced by glutamate since application of total synaptic inhibition uniformly decreased excitability with considerable non-GABAergic inhibitory influences. However, under the conditions of HFD for 15 days, GABAergic influence is robustly increased so that during direct examination before and after BIC application in CVN^{DMV} from HFD animals almost uniformly increased excitability (∼87.5%, Figure 2I). We also emphasize that knock down of $GABA_ARs$ containing the δ-subunit in ChAT-positive neurons eliminated the impact of HFD on BIC-sensitive excitability (Figure 4E). While the intracellular mechanism(s) of this plasticity is still unclear, these experiments provide additional evidence that $GABA_ARs$ containing the δ-subunit are playing a role in the impact of HFD on vagal motor output.

Tonic GABAergic current is persistently active in neurons and has a considerably large influence on neuronal excitability and cardioinhibitory function of CVNs. In this study, we highlight the importance of tonic GABAergic current in CVN^{DMV} and how HFD influences the inhibitory plasticity of this subpopulation of CVNs. Despite a lower abundance in numbers compared to CVN in NA, CVN^{DMV} is long known to regulate heart rate and ventricular contractility.[14] Our findings provide a fundamental understanding to begin elucidating microcircuits that control cardiac vagal motor output, and how these networks are impacted by HFD. This will ultimately contribute to dissecting etiology of cardiovascular diseases associated with HFD intake and

developing treatments targeting $GABA_A$Rs in cardiovascular diseases.

Limitations of the study

Our experimental design in this study did not exclusively examine the role of astrocytes in GABAergic neurotransmission and GABA transporter function in CVN^{DMV}. Further studies are required to confirm roles of astrocytes in GABA neurotransmission in the brainstem and examine whether the increase of tonic GABA current in CVN^{DMV} is solely dependent on postsynaptic plasticity, or if there is a contribution of astrocytic or GABA transporter dysfunction. Although the use of Cs-containing internal solutions limited their influence, we did not directly access the role of metabotropic $GABA_A$Rs in our electrophysiology recording that are worthy of investigation in future studies given the activity of metabotropic $GABA_A$Rs can affect $GABA_A$R desensitization.[81] Our ChAT-δ-null mouse also likely reduced expression of the δ-subunit in NA and other organ projecting populations in DMV. However, our use of a reduced preparation paired with retrograde tracing in the present study limited concern on specificity to DMV. It remains possible that elimination of $GABA_A$Rs containing the δ-subunit in all vagal motor neurons results in improvements in other organ functions, for example gastrointestinal function, and that this improvement was responsibility for the abolishment of the impact of HFD on CVN^{DMV} activity. However, experiments using δ-subunit specific pharmacology provides confidence that $GABA_A$Rs containing the δ-subunit in CVN^{DMV} are impacted by HFD and warrant further investigations. Future *in vivo* studies are also warranted to confirm the role of $GABA_A$Rs containing the δ-subunit in CVN^{DMV}, the impact of HFD on cardiac physiology, and make comparisons between other vagal motor output population.

RESOURCE AVAILABILITY

Lead contact

Further information and requests for resources and reagents should be directed to and will be fulfilled by the lead contact, Carie R. Boychuk (boychukc@missouri.edu).

Materials availability

This study did not generate new unique reagents or mouse lines.

Data and code availability

- The remaining data and information are available within the main text or supplementary information.
- This paper does not report original code.
- Any additional information required regarding data is available from the lead contact upon request.

ACKNOWLEDGMENTS

We would like to thank Raehum Paik, B.S. and Selika Garza, B.S. at The Mouse Genome Engineering and Transgenic Facility at UT Health San Antonio for their help characterizing and managing our transgenic mouse line and Drs. Chiou-Miin Wang and Chun-Liang Chen at the BASiC for their help designing and managing the single-cell mRNA analysis. We also thank Dr. Liliana Espinoza for her technical assistance on this project. This work is supported by R01HL157366 NHLBI to C.R.B.

AUTHOR CONTRIBUTIONS

Conceptualization, Y.B.W. and C.R.B.; methodology, Y.B.W. and C.R.B.; formal analysis, Y.B.W. and C.R.B.; investigation, Y.B.W., and C.R.B.; resources, C.R.B.; data curation, Y.B.W. and K.E.D.; writing – original draft preparation, Y.B.W. and K.E.D.; writing – review & editing, Y.B.W., K.E.D., and C.R.B.; visualization, Y.B.W. and K.E.D.; supervision, C.R.B.; funding acquisition, C.R.B.

DECLARATION OF INTERESTS

The authors declare no competing interests.

STAR★METHODS

Detailed methods are provided in the online version of this paper and include the following:

- KEY RESOURCES TABLE
- EXPERIMENTAL MODEL AND STUDY PARTICIPANT DETAILS
  - Animal
- METHOD DETAILS
  - Retrograde tracing
  - High-fat diet feeding
  - Electrophysiology
  - Single-cell quantitative reverse-transcription PCR
  - Immunohistochemistry
- QUANTIFICATION AND STATISTICAL ANALYSIS

SUPPLEMENTAL INFORMATION

Supplemental information can be found online at https://doi.org/10.1016/j.isci.2025.112268.

Received: March 6, 2024
Revised: December 20, 2024
Accepted: March 18, 2025
Published: March 22, 2025

REFERENCES

1. Fukuda, K., Kanazawa, H., Aizawa, Y., Ardell, J.L., and Shivkumar, K. (2015). Cardiac innervation and sudden cardiac death. Circ. Res. *116*, 2005–2019. https://doi.org/10.1161/circresaha.116.304679.
2. Florea, V.G., and Cohn, J.N. (2014). The Autonomic Nervous System and Heart Failure. Circ. Res. *114*, 1815–1826. https://doi.org/10.1161/CIRCRESAHA.114.302589.
3. Thayer, J.F., and Lane, R.D. (2007). The role of vagal function in the risk for cardiovascular disease and mortality. Biol. Psychol. *74*, 224–242. https://doi.org/10.1016/j.biopsycho.2005.11.013.
4. Ng, G.A. (2014). Vagal modulation of cardiac ventricular arrhythmia. Exp. Physiol. *99*, 295–299. https://doi.org/10.1113/expphysiol.2013.072652.
5. Beske, S.D., Alvarez, G.E., Ballard, T.P., and Davy, K.P. (2002). Reduced cardiovagal baroreflex gain in visceral obesity: implications for the metabolic syndrome. Am. J. Physiol. Heart Circ. Physiol. *282*, H630–H635. https://doi.org/10.1152/ajpheart.00642.2001.
6. Lee, D.Y., Lee, M.Y., Cho, J.H., Kwon, H., Rhee, E.J., Park, C.Y., Oh, K.W., Lee, W.Y., Park, S.W., Ryu, S., and Park, S.E. (2020). Decreased Vagal Activity and Deviation in Sympathetic Activity Precedes Development of Diabetes. Diabetes Care *43*, 1336–1343. https://doi.org/10.2337/dc19-1384.
7. Hartnett, S., Gao, H., Schnack, S., and Li, Y. (2015). Reduced vagal control of the heart in high-fat diet mice: a potential role of increased butyrylcholinesterase. Physiol. Rep. *3*, e12609. https://doi.org/10.14814/phy2.12609.

8. Barzel, B., Weir, J.M., Meikle, P.J., Burke, S.L., Armitage, J.A., and Head, G.A. (2014). Short term fat feeding rapidly increases plasma insulin but does not result in dyslipidaemia. Front. Physiol. *5*, 469. https://doi.org/10.3389/fphys.2014.00469.

9. Armitage, J.A., Burke, S.L., Prior, L.J., Barzel, B., Eikelis, N., Lim, K., and Head, G.A. (2012). Rapid onset of renal sympathetic nerve activation in rabbits fed a high-fat diet. Hypertension *60*, 163–171. https://doi.org/10.1161/hypertensionaha.111.190413.

10. Strain, M.M., Espinoza, L., Fedorchak, S., Littlejohn, E.L., Andrade, M.A., Toney, G.M., and Boychuk, C.R. (2023). Early central cardiovagal dysfunction after high fat diet in a murine model. Sci. Rep. *13*, 6550. https://doi.org/10.1038/s41598-023-32492-w.

11. Standish, A., Enquist, L.W., and Schwaber, J.S. (1994). Innervation of the heart and its central medullary origin defined by viral tracing. Science *263*, 232–234.

12. Standish, A., Enquist, L.W., Escardo, J.A., and Schwaber, J.S. (1995). Central neuronal circuit innervating the rat heart defined by transneuronal transport of pseudorabies virus. J. Neurosci. *15*, 1998–2012.

13. Strain, M.M., Conley, N.J., Kauffman, L.S., Espinoza, L., Fedorchak, S., Martinez, P.C., Crook, M.E., Jalil, M., Hodes, G.E., Abbott, S.B.G., et al. (2024). Dorsal motor vagal neurons can elicit bradycardia and reduce anxiety-like behavior. iScience *27*, 109137. https://doi.org/10.1016/j.isci.2024.109137.

14. Gourine, A.V., Machhada, A., Trapp, S., and Spyer, K.M. (2016). Cardiac vagal preganglionic neurones: An update. Auton. Neurosci. *199*, 24–28. https://doi.org/10.1016/j.autneu.2016.06.003.

15. Loewy, A.D., and Spyer, K.M. (1990). Vagal preganglionic neurons. In Central Regulation of Autonomic Functions, A.D. Loewy and K.M. Spyer, eds. (Oxford University Press), pp. 68–87.

16. Machhada, A., Hosford, P.S., Dyson, A., Ackland, G.L., Mastitskaya, S., and Gourine, A.V. (2020). Optogenetic Stimulation of Vagal Efferent Activity Preserves Left Ventricular Function in Experimental Heart Failure. JACC. Basic Transl. Sci. *5*, 799–810. https://doi.org/10.1016/j.jacbts.2020.06.002.

17. Mastitskaya, S., Marina, N., Gourine, A., Gilbey, M.P., Spyer, K.M., Teschemacher, A.G., Kasparov, S., Trapp, S., Ackland, G.L., and Gourine, A.V. (2012). Cardioprotection evoked by remote ischaemic preconditioning is critically dependent on the activity of vagal pre-ganglionic neurones. Cardiovasc. Res. *95*, 487–494. https://doi.org/10.1093/cvr/cvs212.

18. Blake, C.B., and Smith, B.N. (2012). Insulin reduces excitation in gastric-related neurons of the dorsal motor nucleus of the vagus. Am. J. Physiol. Regul. Integr. Comp. Physiol. *303*, R807–R814. https://doi.org/10.1152/ajpregu.00276.2012.

19. Boychuk, C.R., Gyarmati, P., Xu, H., and Smith, B.N. (2015). Glucose sensing by GABAergic neurons in the mouse nucleus tractus solitarii. J. Neurophysiol. *114*, 999–1007. https://doi.org/10.1152/jn.00310.2015.

20. Balfour, R.H., and Trapp, S. (2007). Ionic currents underlying the response of rat dorsal vagal neurones to hypoglycaemia and chemical anoxia. J. Physiol. *579*, 691–702. https://doi.org/10.1113/jphysiol.2006.126094.

21. McMenamin, C.A., Travagli, R.A., and Browning, K.N. (2018). Perinatal high fat diet increases inhibition of dorsal motor nucleus of the vagus neurons regulating gastric functions. Neuro Gastroenterol. Motil. *30*, e13150. https://doi.org/10.1111/nmo.13150.

22. Bhagat, R., Fortna, S.R., and Browning, K.N. (2015). Exposure to a high fat diet during the perinatal period alters vagal motoneurone excitability, even in the absence of obesity. J. Physiol. *593*, 285–303. https://doi.org/10.1113/jphysiol.2014.282806.

23. Clyburn, C., Travagli, R.A., and Browning, K.N. (2018). Acute high-fat diet upregulates glutamatergic signaling in the dorsal motor nucleus of the vagus. Am. J. Physiol. Gastrointest. Liver Physiol. *314*, G623–G634. https://doi.org/10.1152/ajpgi.00395.2017.

24. Basalay, M.V., Mastitskaya, S., Mrochek, A., Ackland, G.L., Del Arroyo, A.G., Sanchez, J., Sjoquist, P.O., Pernow, J., Gourine, A.V., and Gourine, A. (2016). Glucagon-like peptide-1 (GLP-1) mediates cardioprotection by remote ischaemic conditioning. Cardiovasc. Res. *112*, 669–676. https://doi.org/10.1093/cvr/cvw216.

25. d'Almeida, O.C., Violante, I.R., Quendera, B., Moreno, C., Gomes, L., and Castelo-Branco, M. (2020). The neurometabolic profiles of GABA and Glutamate as revealed by proton magnetic resonance spectroscopy in type 1 and type 2 diabetes. PLoS One *15*, e0240907. https://doi.org/10.1371/journal.pone.0240907.

26. Sa, M., Yoo, E.-S., Koh, W., Park, M.G., Jang, H.-J., Yang, Y.R., Bhalla, M., Lee, J.-H., Lim, J., Won, W., et al. (2023). Hypothalamic GABRA5-positive neurons control obesity via astrocytic GABA. Nat. Metab. *5*, 1506–1525. https://doi.org/10.1038/s42255-023-00877-w.

27. Saxena, N.C., and Macdonald, R.L. (1994). Assembly of GABAA receptor subunits: role of the delta subunit. J. Neurosci. *14*, 7077–7086.

28. Mody, I. (2001). Distinguishing between GABA(A) receptors responsible for tonic and phasic conductances. Neurochem. Res. *26*, 907–913. https://doi.org/10.1023/a:1012376215967.

29. Vithlani, M., Terunuma, M., and Moss, S.J. (2011). The dynamic modulation of GABA(A) receptor trafficking and its role in regulating the plasticity of inhibitory synapses. Physiol. Rev. *91*, 1009–1022. https://doi.org/10.1152/physrev.00015.2010.

30. Gao, H., and Smith, B.N. (2010). Tonic GABAA receptor-mediated inhibition in the rat dorsal motor nucleus of the vagus. J. Neurophysiol. *103*, 904–914. https://doi.org/10.1152/jn.00511.2009.

31. Thomas, P., Mortensen, M., Hosie, A.M., and Smart, T.G. (2005). Dynamic mobility of functional GABAA receptors at inhibitory synapses. Nat. Neurosci. *8*, 889–897. https://doi.org/10.1038/nn1483.

32. Boychuk, C.R., Halmos, K.C., and Smith, B.N. (2015). Diabetes induces GABA receptor plasticity in murine vagal motor neurons. J. Neurophysiol. *114*, 698–706. https://doi.org/10.1152/jn.00209.2015.

33. Travagli, R.A., Hermann, G.E., Browning, K.N., and Rogers, R.C. (2006). Brainstem circuits regulating gastric function. Annu. Rev. Physiol. *68*, 279–305. https://doi.org/10.1146/annurev.physiol.68.040504.094635.

34. Semyanov, A., Walker, M.C., Kullmann, D.M., and Silver, R.A. (2004). Tonically active GABA A receptors: modulating gain and maintaining the tone. Trends Neurosci. *27*, 262–269. https://doi.org/10.1016/j.tins.2004.03.005.

35. Brickley, S.G., and Mody, I. (2012). Extrasynaptic GABAA Receptors: Their Function in the CNS and Implications for Disease. Neuron *73*, 23–34. https://doi.org/10.1016/j.neuron.2011.12.012.

36. Sun, M.Y., Shu, H.J., Benz, A., Bracamontes, J., Akk, G., Zorumski, C.F., Steinbach, J.H., and Mennerick, S.J. (2018). Chemogenetic Isolation Reveals Synaptic Contribution of δ GABA(A) Receptors in Mouse Dentate Granule Neurons. J. Neurosci. *38*, 8128–8145. https://doi.org/10.1523/jneurosci.0799-18.2018.

37. Lee, V., and Maguire, J. (2014). The impact of tonic GABAA receptor-mediated inhibition on neuronal excitability varies across brain region and cell type. Front. Neural Circuits *8*, 3. https://doi.org/10.3389/fncir.2014.00003.

38. Babic, T., Browning, K.N., and Travagli, R.A. (2011). Differential organization of excitatory and inhibitory synapses within the rat dorsal vagal complex. Am. J. Physiol. Gastrointest. Liver Physiol. *300*, G21–G32. https://doi.org/10.1152/ajpgi.00363.2010.

39. Sente, A., Desai, R., Naydenova, K., Malinauskas, T., Jounaidi, Y., Miehling, J., Zhou, X., Masiulis, S., Hardwick, S.W., Chirgadze, D.Y., et al. (2022). Differential assembly diversifies GABAA receptor structures and signalling. Nature *604*, 190–194. https://doi.org/10.1038/s41586-022-04517-3.

40. Levitan, E.S., Schofield, P.R., Burt, D.R., Rhee, L.M., Wisden, W., Köhler, M., Fujita, N., Rodriguez, H.F., Stephenson, A., Darlison, M.G., et al. (1988). Structural and functional basis for GABAA receptor heterogeneity. Nature *335*, 76–79. https://doi.org/10.1038/335076a0.

41. Stell, B.M., Brickley, S.G., Tang, C.Y., Farrant, M., and Mody, I. (2003). Neuroactive steroids reduce neuronal excitability by selectively enhancing tonic inhibition mediated by delta subunit-containing GABAA receptors.

Proc. Natl. Acad. Sci. USA *100*, 14439–14444. https://doi.org/10.1073/pnas.2435457100.

42. Bai, D., Zhu, G., Pennefather, P., Jackson, M.F., MacDonald, J.F., and Orser, B.A. (2001). Distinct functional and pharmacological properties of tonic and quantal inhibitory postsynaptic currents mediated by gamma-aminobutyric acid(A) receptors in hippocampal neurons. Mol. Pharmacol. *59*, 814–824. https://doi.org/10.1124/mol.59.4.814.
43. Yeung, J.Y.T., Canning, K.J., Zhu, G., Pennefather, P., MacDonald, J.F., and Orser, B.A. (2003). Tonically activated GABAA receptors in hippocampal neurons are high-affinity, low-conductance sensors for extracellular GABA. Mol. Pharmacol. *63*, 2–8. https://doi.org/10.1124/mol.63.1.2.
44. Johnson, S.W., and Seutin, V. (1997). Bicuculline methiodide potentiates NMDA-dependent burst firing in rat dopamine neurons by blocking apamin-sensitive Ca2+-activated K+ currents. Neurosci. Lett. *231*, 13–16. https://doi.org/10.1016/s0304-3940(97)00508-9.
45. Debarbieux, F., Brunton, J., and Charpak, S. (1998). Effect of bicuculline on thalamic activity: a direct blockade of IAHP in reticularis neurons. J. Neurophysiol. *79*, 2911–2918. https://doi.org/10.1152/jn.1998.79.6.2911.
46. Khawaled, R., Bruening-Wright, A., Adelman, J.P., and Maylie, J. (1999). Bicuculline block of small-conductance calcium-activated potassium channels. Pflugers Arch. *438*, 314–321. https://doi.org/10.1007/s004240050915.
47. Stocker, M., Krause, M., and Pedarzani, P. (1999). An Apamin-Sensitive Ca^{2+}-activated K^{+} Current in Hippocampal Pyramidal Neurons. Proc. Natl. Acad. Sci. USA *96*, 4662–4667.
48. de Lartigue, G., Barbier de la Serre, C., Espero, E., Lee, J., and Raybould, H.E. (2011). Diet-induced obesity leads to the development of leptin resistance in vagal afferent neurons. Am. J. Physiol. Endocrinol. Metab. *301*, E187–E195. https://doi.org/10.1152/ajpendo.00056.2011.
49. Kentish, S., Li, H., Philp, L.K., O'Donnell, T.A., Isaacs, N.J., Young, R.L., Wittert, G.A., Blackshaw, L.A., and Page, A.J. (2012). Diet-induced adaptation of vagal afferent function. J. Physiol. *590*, 209–221. https://doi.org/10.1113/jphysiol.2011.222158.
50. Korsak, A., Kellett, D.O., Aziz, Q., Anderson, C., D'Souza, A., Tinker, A., Ackland, G.L., and Gourine, A.V. (2023). Immediate and sustained increases in the activity of vagal preganglionic neurons during exercise and after exercise training. Cardiovasc. Res. *119*, 2329–2341. https://doi.org/10.1093/cvr/cvad115.
51. Gao, H., and Smith, B.N. (2010). Zolpidem modulation of phasic and tonic GABA currents in the rat dorsal motor nucleus of the vagus. Neuropharmacology *58*, 1220–1227. https://doi.org/10.1016/j.neuropharm.2010.03.003.
52. Fox, E.A., and Powley, T.L. (1985). Longitudinal columnar organization within the dorsal motor nucleus represents separate branches of the abdominal vagus. Brain Res. *341*, 269–282. https://doi.org/10.1016/0006-8993(85)91066-2.
53. Tao, J., Campbell, J.N., Tsai, L.T., Wu, C., Liberles, S.D., and Lowell, B.B. (2021). Highly selective brain-to-gut communication via genetically defined vagus neurons. Neuron *109*, 2106–2115.e4. https://doi.org/10.1016/j.neuron.2021.05.004.
54. Davis, S.F., Derbenev, A.V., Williams, K.W., Glatzer, N.R., and Smith, B.N. (2004). Excitatory and inhibitory local circuit input to the rat dorsal motor nucleus of the vagus originating from the nucleus tractus solitarius. Brain Res. *1017*, 208–217. https://doi.org/10.1016/j.brainres.2004.05.049.
55. Gao, H., Glatzer, N.R., Williams, K.W., Derbenev, A.V., Liu, D., and Smith, B.N. (2009). Morphological and electrophysiological features of motor neurons and putative interneurons in the dorsal vagal complex of rats and mice. Brain Res. *1291*, 40–52. https://doi.org/10.1016/j.brainres.2009.07.024.
56. Ade, K.K., Janssen, M.J., Ortinski, P.I., and Vicini, S. (2008). Differential tonic GABA conductances in striatal medium spiny neurons. J. Neurosci. *28*, 1185–1197. https://doi.org/10.1523/jneurosci.3908-07.2008.
57. Boychuk, C.R., and Smith, B.N. (2016). Glutamatergic drive facilitates synaptic inhibition of dorsal vagal motor neurons after experimentally induced diabetes in mice. J. Neurophysiol. *116*, 1498–1506. https://doi.org/10.1152/jn.00325.2016.
58. Clyburn, C., and Browning, K.N. (2021). Glutamatergic plasticity within neurocircuits of the dorsal vagal complex and the regulation of gastric functions. Am. J. Physiol. Gastrointest. Liver Physiol. *320*, G880–G887. https://doi.org/10.1152/ajpgi.00014.2021.
59. Bélanger, M., Allaman, I., and Magistretti, P.J. (2011). Brain energy metabolism: focus on astrocyte-neuron metabolic cooperation. Cell Metab. *14*, 724–738. https://doi.org/10.1016/j.cmet.2011.08.016.
60. Minelli, A., DeBiasi, S., Brecha, N.C., Zuccarello, L.V., and Conti, F. (1996). GAT-3, a high-affinity GABA plasma membrane transporter, is localized to astrocytic processes, and it is not confined to the vicinity of GABAergic synapses in the cerebral cortex. J. Neurosci. *16*, 6255–6264. https://doi.org/10.1523/jneurosci.16-19-06255.1996.
61. Matott, M.P., Kline, D.D., and Hasser, E.M. (2017). Glial EAAT2 regulation of extracellular nTS glutamate critically controls neuronal activity and cardiorespiratory reflexes. J. Physiol. *595*, 6045–6063. https://doi.org/10.1113/jp274620.
62. Martinez, D., and Kline, D.D. (2021). The role of astrocytes in the nucleus tractus solitarii in maintaining central control of autonomic function. Am. J. Physiol. Regul. Integr. Comp. Physiol. *320*, R418–R424. https://doi.org/10.1152/ajpregu.00254.2020.
63. Thaler, J.P., Yi, C.-X., Schur, E.A., Guyenet, S.J., Hwang, B.H., Dietrich, M.O., Zhao, X., Sarruf, D.A., Izgur, V., Maravilla, K.R., et al. (2012). Obesity is associated with hypothalamic injury in rodents and humans. J. Clin. Investig. *122*, 153–162. https://doi.org/10.1172/JCI59660.
64. Zhang, Y., Reichel, J.M., Han, C., Zuniga-Hertz, J.P., and Cai, D. (2017). Astrocytic Process Plasticity and IKKbeta/NF-kappaB in Central Control of Blood Glucose, Blood Pressure, and Body Weight. Cell Metab. *25*, 1091–1102.e1094. https://doi.org/10.1016/j.cmet.2017.04.002.
65. Ellacott, K.L.J. (2022). Astrocytes in neural circuits controlling appetite and food intake. Current Opinion in Endocrine and Metabolic Research *22*, 100313. https://doi.org/10.1016/j.coemr.2021.100313.
66. Clyburn, C., Carson, K.E., Smith, C.R., Travagli, R.A., and Browning, K.N. (2023). Brainstem astrocytes control homeostatic regulation of caloric intake. J. Physiol. *601*, 801–829. https://doi.org/10.1113/JP283566.
67. Beltrán-Castillo, S., Olivares, M.J., Contreras, R.A., Zúñiga, G., Llona, I., von Bernhardi, R., and Eugenín, J.L. (2017). D-serine released by astrocytes in brainstem regulates breathing response to CO2 levels. Nat. Commun. *8*, 838. https://doi.org/10.1038/s41467-017-00960-3.
68. Abramian, A.M., Comenencia-Ortiz, E., Modgil, A., Vien, T.N., Nakamura, Y., Moore, Y.E., Maguire, J.L., Terunuma, M., Davies, P.A., and Moss, S.J. (2014). Neurosteroids promote phosphorylation and membrane insertion of extrasynaptic GABAA receptors. Proc. Natl. Acad. Sci. USA *111*, 7132–7137. https://doi.org/10.1073/pnas.1403285111.
69. Gutiérrez, M.L., Ferreri, M.C., Farb, D.H., and Gravielle, M.C. (2014). GABA-induced uncoupling of GABA/benzodiazepine site interactions is associated with increased phosphorylation of the GABAA receptor. J. Neurosci. Res. *92*, 1054–1061. https://doi.org/10.1002/jnr.23387.
70. Barnard, E.A., Skolnick, P., Olsen, R.W., Mohler, H., Sieghart, W., Biggio, G., Braestrup, C., Bateson, A.N., and Langer, S.Z. (1998). International Union of Pharmacology. XV. Subtypes of gamma-aminobutyric acidA receptors: classification on the basis of subunit structure and receptor function. Pharmacol. Rev. *50*, 291–313.
71. Kasaragod, V.B., Mortensen, M., Hardwick, S.W., Wahid, A.A., Dorovykh, V., Chirgadze, D.Y., Smart, T.G., and Miller, P.S. (2022). Mechanisms of inhibition and activation of extrasynaptic αβ GABAA receptors. Nature *602*, 529–533. https://doi.org/10.1038/s41586-022-04402-z.

72. Marti-Solano, M., Crilly, S.E., Malinverni, D., Munk, C., Harris, M., Pearce, A., Quon, T., Mackenzie, A.E., Wang, X., Peng, J., et al. (2020). Combinatorial expression of GPCR isoforms affects signalling and drug responses. Nature *587*, 650–656. https://doi.org/10.1038/s41586-020-2888-2.

73. Eaton, M.M., Bracamontes, J., Shu, H.J., Li, P., Mennerick, S., Steinbach, J.H., and Akk, G. (2014). γ-aminobutyric acid type A α4, β2, and δ subunits assemble to produce more than one functionally distinct receptor type. Mol. Pharmacol. *86*, 647–656. https://doi.org/10.1124/mol.114.094813.

74. Martenson, J.S., Yamasaki, T., Chaudhury, N.H., Albrecht, D., and Tomita, S. (2017). Assembly rules for GABA(A) receptor complexes in the brain. Elife *6*, e27443. https://doi.org/10.7554/eLife.27443.

75. Boychuk, J.A., Butler, C.R., Halmos, K.C., and Smith, B.N. (2016). Enduring changes in tonic GABAA receptor signaling in dentate granule cells after controlled cortical impact brain injury in mice. Exp. Neurol. *277*, 178–189. https://doi.org/10.1016/j.expneurol.2016.01.005.

76. Zhang, N., Wei, W., Mody, I., and Houser, C.R. (2007). Altered localization of GABA(A) receptor subunits on dentate granule cell dendrites influences tonic and phasic inhibition in a mouse model of epilepsy. J. Neurosci. *27*, 7520–7531. https://doi.org/10.1523/jneurosci.1555-07.2007.

77. Jacob, T.C., Moss, S.J., and Jurd, R. (2008). GABAA receptor trafficking and its role in the dynamic modulation of neuronal inhibition. Nat. Rev. Neurosci. *9*, 331–343. https://doi.org/10.1038/nrn2370.

78. Boychuk, C.R., Smith, K.C., and Smith, B.N. (2017). Functional and molecular plasticity of γ and α1 GABA(A) receptor subunits in the dorsal motor nucleus of the vagus after experimentally induced diabetes. J. Neurophysiol. *118*, 2833–2841. https://doi.org/10.1152/jn.00085.2017.

79. Littlejohn, E.L., and Boychuk, C.R. (2021). Protein Kinase C-Dependent Effects of Neurosteroids on Synaptic GABA(A) Receptor Inhibition Require the δ-Subunit. Front. Physiol. *12*, 742838. https://doi.org/10.3389/fphys.2021.742838.

80. Browning, K.N., and Travagli, R.A. (2011). Plasticity of vagal brainstem circuits in the control of gastrointestinal function. Auton. Neurosci. *161*, 6–13. https://doi.org/10.1016/j.autneu.2010.11.001.

81. Field, M., Dorovykh, V., Thomas, P., and Smart, T.G. (2021). Physiological role for GABAA receptor desensitization in the induction of long-term potentiation at inhibitory synapses. Nat. Commun. *12*, 2112. https://doi.org/10.1038/s41467-021-22420-9.

STAR★METHODS

KEY RESOURCES TABLE

REAGENT or RESOURCE	SOURCE	IDENTIFIER
Antibodies		
Goat-anti ChAT	Millipore	Cat# AB114P; RRID: AB_2313845
Donkey anti goat AF488 plus	Invitrogen	Cat# A38214; RRID: AB_2762838
Donkey anti goat AF568	Invitrogen	Cat# A-11057; RRID: AB_2534104
Chemicals, peptides, and recombinant proteins		
Tetramethylrhodamine-5-(and-6)-isothiocyanate	Invitrogen	T490
Kynurenic acid	Sigma Aldrich	K3375
Bicuculine methiodide	R&D System	2503
SR 95531 hydrobromide (Gabazine)	Tocris Bioscience	1262
Picrotoxin	Tocris Bioscience	1128
AP-5	Hello Bio	HB0225
CNQX	Hello Bio	HB0204
Biocytin	Sigma Aldrich	B4261
Texas Avidin Red	Vector Laboratories	A-2206
Vectashield mounting medium	Vector Laboratories	Cat# H-1000; RRID: AB_2336789
OCT compound	Tissue Plus Fisher Healthcare	4585
Normal donkey serum	Jackson Immuno	Cat# 017-000-121; RRID: AB_2337258
Experimental models: Organisms/strains		
C57BL/6J	Jackson Laboratory	Cat#: #000664; RRID: IMSR_JAX:000664
ChAT-δ-null	In house	Littlejohn & Boychuk[79]
δ*KI	Jackson Laboratory	Cat# 032620; RRID: IMSR_JAX:032620
Oligonucleotides		
Single-cell qRT-PCR Primers		See Table S1
Software and algorithms		
GraphPad	GraphPad	V9
ImageJ	NIH Image	1.52n
pClamp	Axon Instruments	V10.6
Mini Analysis	Synaptosoft	V6.03
Clampfit	Molecular Devices	V10.2
Ocular Image	Photometrics	V2.0
Other		
Normal fat diet 10% kcal from fat	Research Diet	D12450Bi
High fat diet 60% kcal from fat	Research Diet	D12492i
Small animal ventilator	CWE Inc.	SAR-830/AP
Mouse attachment ventilator	CWE Inc.	1201020
Vibratome	Leica	VT1000S
Microscope	Olympus	BX51WI
Borosilicate glass pipette	King Precision Glass	
Pipette puller	Sutter Instruments	P-97
Multiclamp amplifier	Axon Instruments	700B
Digidata analog digital converter	Axon Instruments	1440A
CellsDirect™ One-Step qRT-PCR Kit	Invitrogen	11753–100
BioMark HD MX/HX 12 X 12 microfluidic chip system	Fluidigm Inc.	BMKHDPKG- MH

(*Continued on next page*)

Continued

REAGENT or RESOURCE	SOURCE	IDENTIFIER
Cryostat	Leica	CM1860
Fluorescence microscope	Olympus	BX43
Q Imaging CCD camera	Photometrics	Retina R6

EXPERIMENTAL MODEL AND STUDY PARTICIPANT DETAILS

Animal

All procedures and experiments on animals were approved by the University of Texas Health Science Center at San Antonio (UTHSA; approval number 20210096AR) and University of Missouri Animal Care and Use Committee (MU; 43522). All procedures were performed according to the Guide for the Care and Use of Laboratory Animals and ARRIVE Guidelines. Male mice (8–11 weeks, 24.09 ± 0.62 g at start of diet) were used in the experiments. C57/BL6J, ChAT-δ-null and δ*KI (B6;CBA-*Gabrd*^{em1Menn}/J; 032620; Jackson Laboratory; Bar Harbor, ME) colonies are established in-house at the UTHSA and Dalton Cardiovascular Research Center animal facility. Primers for genotyping of d*KI mice (5′- CCTCATTCTGTCTGCCCTG-3′ and 3′-GACCTTGGCTTTCCGTTTCT-5′) were developed and tissue samples sent to Transnetyx Inc (Cordova, TN) for analysis. Animals were group housed up to five per cage with *ad libitum* access to food and water on a 14:10 light/dark cycle. The number of animals used is reported correspondingly in each figure legend.

METHOD DETAILS

Retrograde tracing

Seven-week-old mice were anesthetized with ketamine/xylazine (100/10 mg/kg, intraperitoneal). For cardiac retrograde tracing, animals were intubated using a small animal ventilator (SAR-830/AP; CWE Inc., Ardmore, PA) equipped with mouse attachment (1201020). Mice were placed in a supine position on a heating pad. A small lateral incision between the second and third ribs of the right rib cages was made to expose the thoracic cavity. 40ul of tetramethylrhodamine-5-(and-6)-isothiocyanate (rhodamine; Invitrogen T490; Waltham, MA) was injected into the pericardial fat pad near the posterior right atrioventricular junction where cardiovagal nerve endings terminate. The incision was closed using suture, and the animals were removed from the ventilator. For gastric retrograde tracing, a laparotomy was performed to expose the stomach. Rhodamine (40 μL) was injected into the muscular layer of ventral stomach wall. After the injection, the abdominal cavity was rinsed with warm saline and gently dried to minimize non-specific labeling. The incision was closed using suture. All animals were returned to their home cage for recovery after surgery and monitored for 3 days. Carprofen (10 mg/kg) and buprenorphine (0.1 mg/kg) were administered as post-operative pain relief.

High-fat diet feeding

Animals were acclimatized to a normal fat diet (NFD; 10% kcal from fat, D12450Bi, Research Diets Inc, New Brunswick, NJ) at 6-weeks-old for a week prior to any experimental procedures. At 7-weeks-old, animals underwent surgery to retrogradely label cardiac vagal motor neurons, followed by a week of recovery. At 8-weeks of age, mice were then randomly assigned into two diet groups, a high fat diet (HFD; (60% kcal from fat, D12492i, Research Diets Inc.) or remained on NFD. Mice were maintained on a 15-day dietary regime before electrophysiological experiments unless otherwise noted. Diet was matched based on protein content. HFD consisted of 20% kcal protein, 60% kcal fat, and 20% carbohydrate, with an energy density of 5.21 kcal/g. NFD consisted of 20% kcal protein, 10% kcal fat, and 70% carbohydrate, with an energy density of 3.82 kcal/g. There was no significant weight gain in mice on HFD by Day 15 (9.64 ± 1.9 % of weight before diet) compared to mice on NFD (5.35 1.5 %; unpaired t-test, p=0.15). Weight gain ranged from 0.87 – 8.79% in mice on NFD and 1.77 – 19.15% in mice on HFD. Mice on HFD did consume significantly more kilocalories daily (11.77 ± 0.42 kcal per day) compared to mice on NFD (10.06 ± 0.65 kcal per day; unpaired t-test, p=0.04) throughout the 15 days examined.

Electrophysiology

Preparation of acute brain slice

Mice were anesthetized with isoflurane to effect (i.e. lack of the tail-pinch reflex response) and decapitated. The brainstem was collected and 300μm thick coronal slices were prepared using a vibratome (VT1000S, Leica Biosystems, Buffalo Grove, IL) in ice-cold artificial cerebrospinal fluid (ACSF) containing (in mM): 124 NaCl, 3 KCl, 26 $NaHCO_3$, 1.4 NaH_2PO_4, 11 D-glucose, 1.3 $CaCl_2$, 1.3 $MgCl_2$ and 1 kynurenic acid (290-305 mOsm; pH 7.3-7.4). Slices were incubated in warmed (30-33°C) ACSF for 20 minutes in a holding chamber, followed by a 30-minute incubation at room temperature. All constituents for ACSF were obtained from Sigma Aldrich. The solution was aerated with carbogen (5% CO_2/95% O_2).

Whole-cell patch-clamp recordings

Brain slices were transferred to a recording chamber and neurons were visualized using an Olympus BX51WI (Melville, NY) microscope. Whole-cell patch-clamp recordings were performed under visual control with infrared illumination and differential interference contrast (IR-DIC). A continuous perfusion of warmed aerated ACSF was maintained throughout recordings. Borosilicate glass pipettes (2-5 M Ω; King Precision Glass, Claremont, CA) were pulled using P-97 instrument (Sutter Instruments) and filled with internal solution prior to recording. A minimum of 10-minutes equilibration period was done before recording. Patch-clamp recordings were acquired using Multiclamp 700B amplifier (Axon Instruments, Molecular Devices, Union City, CA) with DigiData 1440A analog digital converter and pClamp v10.6 (Axon Instruments, Molecular Devices, Union City, CA). Signals acquired at either 2 kHz for current-clamp or 20 kHz for voltage-clamp, and low-pass filtered at 3 kHz.

Voltage-clamp configuration was used to identify GABAergic neutrotransmission inhibitory postsynaptic current (IPSC). Warmed aerated ACSF containing 1mM kynurenic acid was used as perfusate. Glass electrodes were filled with Cs-gluconate internal solution containing (in mM): 130 Cs-gluconate, 1 NaCl, 5 EGTA, 10 HEPES, 1 $MgCl_2$, 1 $CaCl_2$, and 2-3 Mg-ATP (pH 7.1-7.2). Cs^+ was used as the primary cation carrier to block K^+ currents, which allowed consistent voltage clamp at depolarized membrane potentials and diminished any influence of postsynaptic $GABA_BR$ during recordings. Biocytin (0.2% final concentration, Sigma) was added to the internal solution to allow visualization post-recording. Both phasic and tonic inhibitory currents mediated by $GABA_AR$ were examined at a holding potential of 0 mV.

Current clamp recordings were performed to determine neuronal excitability and membrane properties. K-gluconate internal recording solution containing (in mM): 130 K-gluconate, 1 NaCl, 5 EGTA, 10 HEPES, 1 $MgCl_2$, 1 $CaCl_2$, and 2-3 Mg-ATP (pH 7.33-7.39) was used to fill the glass electrodes. Action potential (AP) frequency, resting membrane potential (RMP), and input resistance (IR) were measured. Neurons were clamped at −60 mV to ensure a consistent starting voltage before measuring AP response to 400ms duration depolarizing current pulses with current steps injection (0–300 pA with 50pA interval).

Analysis of recordings was done using Clampfit (Molecular Devices) and Mini Analysis v6.0.3 (Synaptosoft, Decatur, CA) for current and voltage clamp configuration respectively. For voltage clamp experiments, phasic $GABA_AR$ neurotransmission was determined based on analysis of 2-minutes of recording before BIC treatment. All synaptic events were used to assess IPSC frequency, but only single peak events were used to determine IPSC amplitude and decay time. Tonic current amplitudes were determined based on the difference between average holding current in 2-minutes of recording before and after BIC treatment. Tonic currents were normalized to whole-cell capacitance to correct for small differences in cell size and are presented as tonic current density (pA/pF).

Action potential frequency, resting membrane potential (RMP), and input resistance (IR) were measured in current clamp mode. RMP was corrected for liquid junction potential post hoc (−7 mV). IR was measured by injecting current-steps (20 pA, 400 ms). To measure AP response to depolarizing current pulses (400 ms duration) of increasing intensity (from 30 to 210 pA), neurons were clamped at −60 mV, to ensure a consistent starting voltage. Number of AP responses during each depolarizing current step were quantified recorded as a count. Afterhyperpolarization (AHP) amplitude was calculated by measuring the absolute value of the anti-peak amplitude (in mV) of the AP afterhyperpolarization. AHP amplitude was measured using the first evoked AP at the 250pA current injection step for each CVN^{DMV}. All recordings were discarded if series resistance was >25 M Ω or changed by >20% throughout the course of the experiment. Mean series resistance was 12.82±1.07 M Ω.

Drugs preparation

Drugs used in this study included $GABA_AR$ antagonists, bicuculline methiodide (BIC; 30μM; R&D Systems, Minneapolis, MN), SR 95531/gabazine (GBZ; 1μM; Tocris Bioscience, 1262; Bristol, United Kingdom) and picrotoxin (PTX; 100μM; Tocris Bioscience, 1128); $GABA_AR$ agonist, THIP hydrochloride (THIP; 3μM; Tocris Bioscience, 0807); as well as glutamate receptor antagonists, 6-cyano-7-nitroquinoxaline-2,3-dione or cyanquixaline (CNQX; 10 mM, Hello Bio, HB0204; Princeton, NJ) and D-2-amino-5-phosphonopentanoate (AP5; 50 mM, Hello Bio, HB0225). All drugs were made according to manufacturers. All drugs were applied in the perfusate for a minimum of five minutes until a steady state was reached.

Single-cell quantitative reverse-transcription PCR

Rhodamine-labeled CVN^{DMV} were collected after electrophysiological recording by applying negative pressure until the cell cytoplasm was aspirated into the patch pipette. The pipette was slightly elevated, and once the neuron rose with the pipette, negative pressure was increased until the entire cell body was collected. Each collected neuron was transferred into a 200 uL RNAse free PCR tube containing 4μL 2X buffer by breaking the tip of the pipette (<10μL total after pipette aspiration). Patch pipettes lacking the entire cell body were discarded. Two different negative control was also collected: 1) one containing only PCR reagents and 2) another where a pipette filled with internal solution was placed at the surface of the tissue and positive pressure was removed for one minute. Isolated neurons and negative controls were immediately stored at -80°C until processed for single-cell quantitative reverse-transcription PCR (scqRT-PCR).

ScqRT-PCR was performed by UTHSA Bioanalytic and Single-Cell Core (BASiC). In brief, collected cells were thawed and lysed at 75°C for 10 min followed by a treatment with DNase I to remove genomic DNA contamination. RT-PCR then was performed using CellsDirect™ One-Step qRT-PCR Kit (#11753–100, Invitrogen), and a microfluidics device, BioMark HD MX/HX 12 X 12 chip system (Fluidigm Inc., BMKHDPKG- MH; South San Francisco, CA). Semi-nested primers for $GABA_AR$ subunits were designed by UTHSA BASiC using Primer3 software and top 25 primer set candidates underwent *in silico* analysis to select the most optimum sequence. Eight final primers were used to detect $GABA_AR$-α_1 (Table S1). Target genes were amplified using a BioMark HB MX/HX system with

1X SsoFast Eva-Green supermix with low ROX (Bio-Rad, N172-5211; Hercules, CA) and 1X DNA binding dye sample loading reagent (Fluidigm, PN 100-3738). GAPDH and β-actin were used as housekeeping genes. Universal mouse RNA (200 pg) (BioChain, R4334566-1; Newark, CA) was used as a positive control. Human embryonic kidney cells and no template were used as negative controls. PCR products amplification was detected using a Fluidigm BioMark HD with the FlexSix IFC using Delta Gene assays (Fluidigm PN 100-7717 B1). Detection was limited to 40 cycles, and any target that did not reach threshold by 40 cycles was considered non-detectable.

Immunohistochemistry

Biocytin and ChAT colocalization

Brain slices were collected at termination of electrophysiological recording to detect colocalization of biocytin/choline acetyltransferase (ChAT)-positive motor neurons thereby confirming identity as motor efferent neurons. Brain slices were fixed in 4% paraformaldehyde in 0.01 M phosphate-buffered saline (PBS) overnight at 4°C, followed by 30% sucrose for two days. Slices were then mounted in OCT compound (Tissue Plus, Fisher Healthcare, 4585, Houston, TX) and serial coronal sections were taken at 40 μM on a cryostat at -19 degrees (Leica Biosystems, CM 1860). Biocytin-filled neurons were processed via avidin, Texas Red staining (TX Red Avidin D; 1:400; Vector Laboratories, A-2206; Newark, CA). Free floating sections were then immuno-labeled for choline-acetyl transferase (ChAT; goat anti-ChAT; 1:250; Sigma-Aldrich, AB144P; St. Louis, MO) followed by secondary antibodies to donkey anti-goat 488 (Alexa Fluor Plus 488; 1:200; Invitrogen A-11055) for four hours at room temperature, to detect co-labeling of ChAT-positive motor neurons in the DMV.

$GABA_AR$-δ-subunit and ChAT colocalization

To verify $GABA_AR$-δ-subunit knock-out in ChAT-δ-Null mice, animals were first transcardially perfused with 0.01M PBS followed by 4% PFA where they remained overnight. Brains were then cryoprotected in 30% sucrose until they sunk. Brain tissue was blocked to include DMV and sectioned in serial coronal sections (40 μM) on a cryostat at -19 degrees (Leica Biosystems). Immunofluorescent staining was then performed on free floating sections for the detection of ChAT and the $GABA_AR$-δ-subunit. For $GABA_AR$-δ-subunit protein expression was probed with primary antibodies (rabbit anti- $GABA_AR$-δ-subunit; 1:50; PhosphoSolutions 868A-GDN; Denver, CO) overnight at 4 degrees, followed by secondary antibodies (donkey anti-rabbit 488, Alexa Fluor Plus 488, 1:200, Invitrogen A-21206) at four hours at room temperature. ChAT expression was probed as above, with the exclusion that secondaries antibodies were tagged with Alexa Fluor 568 (donkey-anti-goat, Alexa Fluor 568, 1:200, Invitrogen A-10042).

After immunohistochemistry, slices were mounted (Vectashield; Vector Laboratories, H-1000) and coverslipped. Imaging was done with an Olympus microscope (BX43), images were captured with a Q Imaging Retina R6 camera (Photometrics; Tucszon, AZ) and Ocular Image Acquisition Software (Photometrics).

QUANTIFICATION AND STATISTICAL ANALYSIS

For patch-clamp electrophysiology experiments, only one cell per slice, and a maximum of three cells were recorded from one animal. Statistical analyses were performed using GraphPad Prism 9 (GraphPad, La Jolla, CA) Results are reported as mean ± SEM unless otherwise stated. Each statistical method used is reported in figure legends accordingly. Changes in neural excitability were determined by subtracting area under the curve value of treatment from baseline area under the curve (positive value=increase; negative value=decrease; 0=no change). Differences were considered statistically significant if $p \leq 0.05$. * indicates $p \leq 0.05$; ** indicates $p \leq 0.01$, *** indicates $p \leq 0.001$, **** indicates $p \leq 0.0001$.